공학석사 학위논문

Formation of Multifunctional Hydrogels via Enzyme-mediated Crosslinking

효소 매개 가교를 통한 다기능성 하이드로겔 제작

2019년 2월

서울대학교 대학원
협동과정 바이오엔지니어링 과정

김 경 민

ABSTRACT

Formation of Multifunctional Hydrogels via Enzyme-mediated Crosslinking

Kyungmin Kim

Interdisciplinary Program in Bioengineering

The Graduate School of Engineering

Seoul National University

In recent years, several attempts have been made to impart functionality to biomaterials in the field of tissue engineering. In particular, injectable form of hydrogels have many advantages such as ease of handling, in situ crosslinking, and being able to apply in 3D bioprinting applications. In this thesis, we demonstrate the synthesis of chitosan-based hydrogels containing Epigallocatechin gallate (EGCG) through recombinant tyrosinase from Streptomyces avermitilis (SA_Ty) that retains the anti-inflammation ability. Application of chitosan-EGCG (Chitosan-E) in wound healing application confirmed the regulation of the immune reaction due to the radical scavenging ability of hydrogel. Furthermore, we also present the synthesis of 3D printing hydrogel that can be crosslinked by SA-Ty by combining decellularized ECM and hyaluronic acid conjugated tyramine (HA_T).

Keyword: Functional hydrogel, 3D-bioprinting, polyphenol, chitosan, decellularized extracellular matrix, tyrosinase

Student Number: 2017-24546

TABLE OF CONTENTS

ABSTRACT ii
TABLE OF CONTENTS iv
CHAPTER ONE: TYROSINASE-MEDIATED CROSSLINKING OF POLYPHENOL FUNCTIONALIZED CHITOSAN FOR WOUND HEALING HYDROGEL 1

2.1 Introduction 1

2.2 Materials and methods 3

2.2.1 Synthesis of tyrosinase from Streptomyces avermitilis(SA-Ty) 3

2.2.2 Fabrication of chitosan hydrogel based on polyphenol 3

2.2.3 Rheological analysis of hydrogels 4

2.2.4 Measurement of Young's modulus 4

2.2.5 Measurement of the swelling ratio of hydrogels 5

2.2.6 Scanning electron microscope(SEM) analysis 5

2.2.7 Measurement of EGCG releasing profile 6

2.2.8 Radical scavenging assays 6

2.2.9 Cell viability and proliferation test 7

2.2.10 *In vitro*, Anti-bacterial test 8

2.2.11 *In vitro*, Anti-inflammatory effects 8

2.2.12 *In vivo*, Wound healing model 9

2.2.13 Immunohistochemistry 9

2.2.14 Statistical analysis 10

2.3 Results 11

2.3.1 Synthesis and characterization of enzyme-mediated hydrogels 11

2.3.2 Mechanical and physical properties of hydrogels 12

2.3.3 Function of Chitosan-E hydrogels 12

2.3.4 *In vivo*, wound healing model 14

2.4 Discussion 15

CHAPTER TWO: SYNTHESIS OF DECELLULARIZED BRAIN ECM-BASED HYDROGEL FOR 3D-BIOPRINTING 18

3.1 Introduction 18

3.2 Materials and methods 20

3.2.1 Materials 20

3.2.2 Decellularization of porcine brain 20

3.2.3 Synthesis of tyramine-modified hyaluronic acid(HA_T) 21

3.2.4 Preparation of hydrogels 22

3.2.5 Rheological analysis 22

3.2.6 Swelling ratios analysis 23

3.2.7 Scanning electron microscopy(SEM) analysis 23

3.2.8 Measurement of Young's modulus 23

3.2.9 Statistical analysis 24

3.3 Results & Discussion 25

3.3.1 Synthesis and characterization of decellularized ECM-based hydrogel 25

3.3.2 Mechanical and physical properties of hydrogels 25

3.3.3 Further work 26

REFERENCES 27

초록(국문요약) 30

LIST OF FIGURES AND TABLE 31

Figures 31

Figure 2.1 Three main component of tissue engineering 31

Figure 2.2 The overall scheme of polyphenol-functionalized chitosan hydrogels formed via an enzyme reaction 32

Figure 2.3 Mechanism of Chitosan-E hydrogels 33

Figure 2.4 Sol fraction of Chitosan-E hydrogels 34

Figure 2.5 Gelation of Chitosan-E hydrogels 35

Figure 2.6 Rheological analysis of Chitosan-E hydrogels 36

Figure 2.7 Mechanical properties of Chitosan-E hydrogels 37

Figure 2.8 Microstructure of Chitosan-E hydrogels 38

Figure 2.9 Releasing profile and function of hydrogel 39
Figure 2.10 Scheme of anti-bacterial test 40
Figure 2.11 Anti-bacterial ability of hydrogel 41
Figure 2.12 Biocompatibility of hydrogel 42
Figure 2.13 Inflammation modulation ability of hydrogel 43
Figure 2.14 Chitosan-E hydrogels injection model 44
Figure 2.15 Scheme of wound healing model and wound healing process 45
Figure 2.16 Wound closing images and ratio 46
Figure 2.17 Histology images 47
Figure 2.18 Immunohistochemistry of wound healing model 48
Figure 2.19 *In vivo*, vascularization in the wound area 49
Figure 3.1 Scheme for the synthesis of decellularized ECM-based hydrogel 50
Figure 3.2 Decellularization step 51
Figure 3.3 Characterization of decellularized ECM 52
Figure 3.4 Gelation images of decellularized ECM hydrogel 53
Figure 3.5 Rheological analysis of decellularized ECM hydrogel 54
Figure 3.6 Mechanical properties of decellularized ECM-based hydrogel 55
Figure 3.7 Scanning electron microscope image 56
Figure 3.8 Further work 57

Tables 58

Table 3.1 DNA quantification 58
Table 3.2 Young's modulus of decellularized ECM-based hydrogel 59

CHAPTER ONE: TYROSINASE-MEDIATED CROSSLINKING OF POLYPHENOL FUNCTIONALIZED CHITOSAN FOR WOUND HEALING HYDROGEL

2.1 Introduction

Tissue engineering is an interdisciplinary field that aims to restore the damaged tissues or organs by engineering the biological replacements [1]. One of the most important aspect of the tissue engineering is the cells. Cells are single most important components in tissues or organs as some cells, in particular, stem cells, have the capacity to regenerate tissues [2-4] . In addition, upon optimal microenvironmental stimuli, somatic cells can also contribute to the tissue regeneration. Another important aspect to consider in tissue engineering is the scaffold system. Scaffolds may provide mechanical integrity of the cells by providing three-dimensional (3D) microenvironment. Third aspect to consider in tissue engineering is the biological stimuli that can elicit controlled cellular behavior. There are many forms of biological stimuli that have been applied in tissue engineering [5, 6]. These include electrical simulation, biomechanical stimulation, growth factor stimulation, or small molecule stimulation [7-10] . All these biological stimuli affects the behavior of cells through alteration in cell adhesion, differentiation, migration. Our laboratory has been conducting experiments to optimize these three factors for enhanced tissue engineering products. This thesis is an extension of our laboratory's technology that utilized hydrogel-based biomaterials that can be crosslinked by tyrosinase. We aimed

to incorporate biofunctionality via small additive molecules that can be crosslinked during the polymerization step. Several studies have proposed to develop hydrogel that can be applied to various tissue engineering applications by introducing functional groups [11, 12].

Although there are various functional materials, polyphenols are attracting attention recently [13]. That is because polyphenol has an anti-inflammation and immune modulation function due to its role as an antioxidant [14, 15]. We synthesized functional hydrogels by forming covalent bonds between these EGCG monomers and chitosan.

There are many ways to crosslink hydrogel [16]. Among them, the method using an enzyme has an advantage that it can be stable and rapidly crosslinked without controlling the pH or changing the temperature [17]. Therefore, we used recombinant tyrosinase derived from Streptomyces avermitilis to oxidize EGCG to induce binding with chitosan.

2.2 Materials and methods

2.2.1 Synthesis of tyrosinase from Streptomyces avermitilis(SA-Ty)

Recombinant plasmids were constructed in the previous study [18]. Briefly, the recombinant plasmids were transformed into E. coli BL21 (DE3) by heat shock. Then, it was inoculated into 4 mL of Luria-Bertani (LB) broth with proper antibiotics, and cultured in an incubator at 37° C and 200 rpm overnight. Next day, 2 mL of cell culture was transferred into a 1L flask with 200 mL of fresh LB and incubated at 37° C and 200 rpm until the optical density at 600nm (OD 600nm) of the cell culture media reached approximately 0.6 to 0.8. Then, the cells were induced with 0.2 mM IPTG and 1.0 mM CuSO4 and incubated at 18° C at 200 rpm for 20hrs. From the next step, it is essential to adjust the temperature to 4° C. Cell pellets was collected using a centrifuge at 4000 rpm and washed with 5 mL of 50mM Tris-HCl pH 8 buffer twice. The cell was lysated by ultra-sonication. After centrifugation at 16000 rpm for 30 min, soluble fraction was collected and filtered through a syringe filter with 0.2μm Membrane. The expressed enzymes within soluble fraction were purified by the general His-tag purification. The concentration of enzymes was measured by BCA assay.

2.2.2 Fabrication of chitosan hydrogel based on polyphenol

Firstly, 3 %(w/v) glycol chitosan solution was prepared by dissolving 300mg of Glycol chitosan in 10 mL of Deionized water. Then, EGCG monomer was dissolved in DMSO to the desired final concentration. SA-Ty, which was synthesized in

advance was prepared in a 37° C water bath. 3% glycol chitosan, EGCG monomer, and SA-Ty were mixed in a volume ratio of 12: 1: 1. Chitosan-E hydrogel made by incubating these mixed solutions overnight at 37° C.

2.2.3 Rheological analysis of hydrogels

Rheological analysis of Chitosan-E hydrogels was conducted in Anton Paar Korea using rheometer (MCR 302, Measuring cell: P-PTD & H-PTD 200, Measuring System: PP 25, Anton-Paar, Austria). All samples were 8 mm in diameter and 2 mm thick. All experiments were conducted at 37° C and air flow. Firstly, a strain sweep test was performed. It was conducted to evaluate critical strain. When the strain increases, the intersection point of G' and G" is the critical strain. Next, a frequency sweep test was performed. From this result, G' and G" was measured when decreasing frequency from 100 Hz to 0.1 Hz. The strain was fixed at 3 %. Finally, a time sweep test was performed to measure the gelation time. G' and G" were measured for 15 min under constant conditions of 2 % strain.

2.2.4 Measurement of Young’s modulus

Young's modulus was measured by using a UTM. Briefly, all samples were uniformly using a PDMS mold with a diameter of 8mm and a height of 2 mm. Then, samples were pressed at a rate of 1 mm/min of probe speed using a UTM. The Young's modulus was calculated from a linear region of the stress-strain curve (5-15% strain).

2.2.5 Measurement of the swelling ratio of hydrogels

For measuring the swelling ratio, 100 uL of gel solution was prepared on a parafilm in a uniform shape. Briefly, mix the 3% glycol chitosan solution, EGCG monomer, and SA-Ty for each composition. After homogeneous mixing, the mixture was prepared in a uniform shape on parafilm. For making a uniform shape, a 8 mm diameter frame made with PDMS was used. This mixture was incubated at 37 ° C for overnight to complete gelation. After hydrogel was made, it was transferred to Deionized water and swelled sufficiently at 37° C. The swelled hydrogel was frozen in a deep freezer after weighing and then lyophilized. The swelling ratio of Chitosan-E hydrogels was measured by the following equations.

$$\text{Swelling ratio} = \frac{W_S - W_D}{W_D}$$

2.2.6 Scanning electron microscope(SEM) analysis

For observing the internal structure of hydrogel, SEM analysis was performed. Firstly, samples were made using a PDMS mold and swelled enough in Deionized water. Then, all samples were lyophilized and sliced using a blade into horizontally to internal analysis structure and mounted on SEM mounts with carbon tape. Before the measurement, the samples were coated with platinum/palladium for 120 seconds in vacuum. The image was observed by JSM-7610F Scanning Electron Microscope (JEOL USA, Inc.) at 10 μA and 10 kV.

2.2.7 Measurement of EGCG releasing profile

To confirm the release of EGCG, the releasing amount of EGCG was measured using Folin & Ciocalteu's phenol reagent. Chitosan-E hydrogels was made the manner described above. Then, it was soaked in 1 mL of DI water, and the sample was collected every day and quantified at once. Briefly, 5 mg of catechin conjugate was dissolved in 10 mL of DI water. 1 mL of this solution was added to a vial and diluted with 5 mL of DI water. 1 mL of Folin & Ciocalteu's phenol reagent was added, and the mixture was shaken. After 3 min, 3 mL of 10.75 wt% sodium carbonate was added, and the mixture was stored in the dark for 3 h with intermittent shaking. At the end of the process, the absorbance of the final solution was measured at 760 nm against a solution prepared from a blank polymer. The degree of functionalization with catechin was determined by comparing the absorbance with a calibration curve developed from native catechin.

2.2.8 Radical scavenging assays

2,2-Diphenyl-1-picrylhydrazyl (DPPH) assay was performed to measure the radical scavenging ability of EGCG released from the hydrogel. Colorimetric changes of DPPH measured it. 100mM Tris-HCl pH 7.4 buffer, in which each sample was embedded for one day, was used for the measurement. Briefly, 12 mL of 0.1 mM DPPH solution with methanol was made. Then, 100 uL of the sample solution was transferred into a 2 mL tube, and we add 100 uL of the prepared 0.1mM DPPH solution to all the tubes. Next, incubate all the tubes in the dark for 30 minutes at room temperature. After 30 minutes, transfer the final solution into 96-well plate and

read absorbance at 517nm with UV-spectroscopy (TECAN infinite m200 pro, Switzerland). The percentage of scavenging radical was calculated following the equation.

$$\text{Percentage of scavenging radical } = \left(\text{Abs. of blank} - \frac{Abs.of\ sample}{Abs.of\ blank}\right) \times 100$$

2.2.9 Cell viability and proliferation test

Firstly, the cell viability and proliferation of Chitosan-E hydrogels was measured using Prestoblue Cell Viability Reagent (Thermo Fisher Scientific) following the manufacturer's instructions. C2C12 cells were cultured in each well of 96-well cell culture plate at a concentration of 1 x 104 cells per well with each hydrogel embedded growth medium. To make the complete growth medium, add the following components to the base medium: fetal bovine serum to a final concentration of 10%, L-glutamine 1%, Penicillin-streptomycin 1%. It was measured daily from day 0 to day 3. Briefly, after washing each well with PBS, incubate with 100ul of media which is mixed with a prestoblue reagent at 9: 1 for 30min. Then, the fluorescence intensity of collected media was quantified using UV-spectroscopy (TECAN infinite m200 pro, Switzerland). Then, all samples were normalized at day 0 fluorescence intensity. Secondly, at day 3, each well was stained with live and dead cell assay. Live and dead cell number and ratio was quantified, and the stained well was imaged with EVOS Cell imaging Systems (Thermo Fisher)

2.2.10 *In vitro*, Anti-bacterial test

For verifying the anti-bacterial effect of EGCG, the following experiment was conducted. First, the E. coli was inoculated into 4 mL of LB Broth with the appropriate antibiotic. Then incubate at 37 ° C overnight in a shaking incubator. At the same time, prepare LB agar gel for culturing E. coli. Briefly,

LB agar gel was prepared by appropriately mixing 7.5 g of agarose and 5 g of LB Broth in 200 mL of di-water. After that, it was sealed and autoclaved. After autoclaving, it is poured into a 100-pie petri dish and allowed to cool down. Also, the hydrogel was prepared as described previously. On the next day, the solution in which E. coli was cultured was transferred to 200 ul in the prepared agar gel and spread until it was dried. After drying, the prepared hydrogel was placed on agar gel at an appropriate distance and cultured for 9 hours. There are two methods for quantifying the anti-bacterial effect. First, it was quantified by calculating the ratio of the area in which E. coli did not grow around the gel. After then, the hydrogel was immersed in fresh LB broth and incubated for 3 hours. OD value of this solution was measured and quantified.

2.2.11 *In vitro*, Anti-inflammatory effects

To demonstrate anti-inflammatory effects *in vitro*, the amount of tissue necrosis factor alpha(TNF-α) from RAW 264.7 cells was quantified. RAW 264.7 cells were cultured on 96-well cell culture plate (cell density: 1 x 104 cells/ well) with each hydrogel embedded growth medium. To make the complete growth medium, add the following components to the base medium: fetal bovine serum to a final

concentration of 10%, L-glutamine 1%, Penicillin-streptomycin 1%. Then, 100 ng/mL of lipopolysaccharide (LPS) was added in each well to stimulate immune reactions. After 24 hours of stimulation, the cell culture supernatant was collected, and the amount of TNF-α was measured using a Mouse TNF-alpha ELISA Complete Kit (KOMAbiotech, Korea).

2.2.12 *In vivo*, Wound healing model

In vivo, the hydrogel was applied to a wound healing model to confirm its functionality. Animal experiments were performed using protocols approved by the Seoul National University Institutional Animal Care and Use Committees. BALB/C mice (female, age 8 weeks, weighing 20~25 g) were purchased from Orient Bio (Orient Bio Inc, Seongnam, Korea). All mice were anesthetized with respiratory anesthetics (Isoflurane during the experiment. First, the anesthetized mice were laid down and punched through the skin using an 8 mm bio-punch. The experimental groups were PBS treated, chitosan hydrogel containing no EGCG using glutaraldehyde, and hydrogel containing 3 mM and 11 mM of EGCG. Samples were collected on day 6, day 10, day 14, and day 21, and H & E staining was carried out.

2.2.13 Immunohistochemistry

Immunohistochemistry was performed to verify the anti-inflammation effect of the hydrogel in samples obtained from in vivo experiments. It was conducted using MOMA-2(Abcam, ab33451), which can stain macrophages and monocytes. Staining was done on day 6 of the Wound model and day 2 of the subcutaneous injection

model.

2.2.14 Statistical analysis

All data are expressed as mean and standard deviation (SD). Statistical significance was evaluated by Student's t-test with *P < 0.05, **P < 0.01, or *** < 0.001

2.3 Results

2.3.1 Synthesis and characterization of enzyme-mediated hydrogels

Chitosan-E hydrogels were fabricated by simple mixing of chitosan, EGCG, and SA-Ty. EGCE provides phenolic groups that enables it to function as crosslinakable moiety upon tyrosinase activation. Therefore, in order to observe the effects of EGCG on hydrogel crosslinking (i.e., physical properties of hydrogel), we prepared Chitosan-E hydrogel with varying amount of final EGCG concentration at 3 mM, 7 mM, and 11 mM. In order to obtain 3 mM, 7mM, and 11 mM Chitosan-E hydrogel, EGCG monomers were dissolved in DMSO at concentration of 42mM, 98mM, and 154mM, respectively. In addition, EGCG solutions were then mixed with glycol chitosan(3% w/v) at 12:1 volume ratio. Finally, tyrosinase (10 μL) was added to 130 μL of chitosan/EGCG mixture for a final concentration of 7 uM. Chitosan-E hydrogels with varying amount of EGCG were crosslinked in the presence of tyrosinase overnight at 37 ° C overnight to complete gelation. After the complete gelation step, Chitosan-E hydrogels were immersed in a NaCl solution which interferes with the electrostatic interaction and weighed to quantify the sol fraction changes of the hydrogel. (Fig. 2.3). Electrostatic interaction may be unrelated in gelation because the sol fraction did not change when compared to the gel immersed in DW. The results of the experiment with hydrogel immersed in Triton-X demonstrate that hydrophobic interaction and hydrophilic interaction are also unrelated in gelation.

2.3.2 Mechanical and physical properties of hydrogels

To measure the gelation kinetic, we permed the tilting experiment for every 30 min to observe the gelation progression. Our observation indicated that 3 hours under oxygen-contactable 37 ° C was sufficient to induce non-tiling condition of Chitosan-E hydrogel. In addition, we examined the initial gelation behavior through rheology analysis. As a result of the time sweep test under 2% strain condition, there is no difference gelation time according to EGCG concentration. To characterize mechanical properties of the hydrogels, we analyzed compressive modulus, loss modulus, and storage modulus by Universal Testing System (UTM) and rheometer. All of the hydrogels used in the experiment were crosslinked sufficiently at 37 ° overnight. In the frequency sweep test, we confirmed that the storage modulus(G') was stably higher than loss modulus (G") at a frequency of 0.1 to 15 Hz. Through the strain sweep test, we verified that as the concentration of EGCG increases, the hydrogel becomes brittle and the gel structure changes at lower strain values. With the same trend as previous data, the higher the concentration of EGCG, the higher Young's modulus and the lower the selling ratio. As a result of observing the microstructure of the hydrogel through a Scanning Electron Microscope (SEM) displayed similar structures among all hydrogels.

2.3.3 Function of Chitosan-E hydrogels

Next, we verified the function of the Chitosan-E. First, the EGCG release of the hydrogel was verified because its function is given by the EGCG. We quantified EGCG using Folin & Ciocalteu's phenol reagent and confirmed that it was burst

releasing within the first 3 days. That is because unreacted EGCG monomer is released. We verified that the 11 mM hydrogel releasing the most EGCG has the highest radical scavenging ability through the DPPH assay. This released EGCG has lower radical scavenging ability compared to the same amount of EGCG monomer. The reason for that, EGCG was oxidized during the gelation process and lost its function as an anti-oxidant. To confirm the radical scavenging ability of these hydrogels, we measured the amount of TNF-α of RAW 264.7 cells supernatant cultured with hydrogel embedded medium. Lipopolysaccharide (LPS) induced RAW cells, and we confirmed that TNF-a release was regulated as the concentration of EGCG increased. These results demonstrate that Chitosan-E hydrogels has anti-inflammation effects. When the cell viability test was performed before the *in vivo* experiment, it was also confirmed that there was no difference from the blank medium used for the control.

Next, the immune modulation function of the hydrogel was verified *in vivo*. We injected the gel solution into mice subcutaneous and collected the mice skins on the 2nd day. As a result of immunostaining the samples, the PBS group showed a similar staining area when compared to the native group. In contrast, inflammation was observed in the 0 mM group using glutaraldehyde, and the other hydrogel injected group. The highest inflammation in the 0 mM group was estimated due to the glutaraldehyde injected together. Similar to *in vitro* results, the higher the concentration of EGCG, the higher the ability of the hydrogel to regulate inflammation.

2.3.4 *In vivo*, wound healing model

The radical scavenging ability of EGCG and the role of antioxidant in burst releasing for the first 3 days were applied to *in vivo* wound healing model. Wound healing, as seen in fig. is a process of wound contraction after inflammation reaction and granulation tissue formation after injury. Therefore, hydrogels are expected to regulate the early inflammation process. There was no significant difference when the closing ratio was measured through the image of the wound healing model. After the experiment, the samples collected on the 6th, 10th, 14th and 21st day were observed by H & E staining. Also, the samples of day 6 were immuno-stained with MOMA-2, and the inflammation was quantified as MOMA-2 stained area ratio. Similar to *in vitro* data, the higher the EGCG concentration, the greater the ability to control inflammation. However, in the PBS group, a slight wound inflammation was observed, unlike the subcutaneous model.

2.4 Discussion

Chitosan, the backbone of our hydrogel, is a biodegradable and bioadhesive materials. Also, It has been shown that chitosan is non-toxic and tissue compatible in a range of toxicity tests. We used glycol chitosan to ensure better solubility in water. Chitosan was dissolved in 1%, 2%, 3% of deionized water and 3% chitosan hydrogel had proper physical properties to maintain its shape. In other words, it was confirmed that 1% and 2% hydrogel did not uniformly gelation. The final concentration of EGCG in the prepared 3% chitosan solution was adjusted to 3 mM, 7 mM, 11 mM and then cross-linked with SA_Ty. The most critical factor in hydrogel synthesis is the oxidation of EGCG. Therefore, gelation takes more than 3 hours to oxidize EGCG through tyrosinase. The hydrogels used in the experiment were all made to be 37° C overnight in order to maintain constant conditions. The gelation mechanism can be explained in two mechanisms by the generation of conjugation bonds between chitosan and EGCG.

First, the enzyme-mediated mechanism is that enzymes such as tyrosinase and laccase oxidizes EGCG under oxygen-mediated conditions and forms a conjugation bond with chitosan. EGCG is highly reactive with tyrosinase so, is well known as a competitive inhibitor. EGCG molecules form radical formation through the quinone form through the oxidation process. This form can make covalent bonds with nucleophilic amine groups of chitosan through Schiff-base reaction and Michael-type reaction without the help of enzymes. These quinone forms can also react with another quinone to form oligomers, which can be used as crosslinkers of various lengths in gelation reactions. The other mechanism is the free radical reaction. The free radicals produced by oxidation of tyrosinase can attack the hydroxyl group,

amino group, and α-methylene group of chitosan. As a result, chitosan can form three types of macromolecular chitosan radicals that can be covalently bonded to polyphenols. We conducted experiments to support these mechanisms. In order to demonstrate this mechanism, the existence of binding involved in the hydrogel formation was confirmed by the sol fraction. These results suggest that oxidation of EGCG is a significant factor in gelation. Also, It demonstrates that Hydrophobic interaction and hydrophilic interaction are also unrelated in gelation.

Properties of Chitosan-E hydrogels were measured by various methods. As expected, the higher the concentration of EGCG, the higher the overall physical properties. That indicates that the higher the concentration of EGCG in the hydrogel, the more crosslinking takes place. Also, it can be seen that the higher the concentration of EGCG, the higher the amount of released EGCG. From this point of view, it can be expected that the hydrogel of 11 mM has the highest immunoregulatory function. That was demonstrated by TNF secretion in Raw cells in vitro. Based on the functional and physical properties of the hydrogel, it was judged to be suitable for the wound healing model.

The in vivo results confirm the functionality of the Chitosan-E hydrogels. The subcutaneous injection model and the wound healing model reveal the inflammatory control function of Chitosan-E hydrogels. First, the subcutaneous injection model shows the highest MOMA-2 staining area in the Chitosan hydrogel made from glutaraldehyde. That can be attributed to the effects of glutaraldehyde and chitosan. Moreover, the higher the concentration of EGCG, the less the inflammatory reaction is due to the hydrogel. The wound healing model also showed the above pattern. One difference is that there is a constant level of MOMA-2 stained area in the PBS group due to wound inflammation. Analysis of the 21 st samples by

H & E staining showed that wound regeneration was effectively caused by inflammation control as previously mentioned, and thus the number of new blood vessels was higher.

From these results, we suggest that Chitosan-E hydrogels is a superior material for bioengineering. Also, we expect to make various attempts through the functionality of this material in the future. For example, It can be used for diseases that are critical for inflammatory reactions.

CHAPTER TWO: SYNTHESIS OF DECELLULARIZED BRAIN ECM-BASED HYDROGEL FOR 3D-BIOPRINTING

3.1 Introduction

In biology, the extracellular matrix (ECM) is a three-dimensional network such as collagen and glycoproteins, that provide structural support of surrounding cells. Also, ECM actively participate in the regulation of cell functions such as proliferation and homeostasis. However, in order for ECM to be applied to allogeneic and xenogeneic recipients, removal of the cell membrane and tissue related cellular components is a necessary process [19]. This is because xenogeneic cells and xenogeneic antigens are recognized by the host as exogenous, leading to adverse inflammatory or immune rejection responses [20, 21]. For this reason, a method of harvesting only ECM components has been developed, such as the decellularization. For over a decade, the hydrogel derived from the extracellular matrix (ECM) of decellularized tissues has been getting attention [19, 22, 23]. One of the clear advantages of utilizing decellularized ECM the hydrogel formation is that the hydrogel can retain biological functionality of ECM. ECM from decellularized tissue may provide cellular adhesion sites and molecular affinity to tissue-specific growth factors, there by mimicking native tissue ECM microenvironment. In particular, Elisseeff and colleagues have created hydrogel composed of pulverized cartilage tissues and PEG-hydrogel. This is tissue-specific hydrogel resulted in microenvironment that is conducive for chondrogenic differentiation of stem cells [24, 25]. In recent years, an

injectable hydrogel composed of decellularized hydrogels has been reported. Therefore we hypothesize that the application or incorporation of decellularized ECM into the 3D bioprinting hydrogel may provide suitable tissue-specific microenvironment [26, 27].

3D printing has been actively studied in the field of tissue engineering [28-32]. The advantage of 3D printing is that it enables us to fabricate patient-specific or on-demand scaffold fabrication. In the field of tissue engineering, biocompatible and polyester-based polymers, such as PLC or PLGA, are heavily utilized in extrusion-based 3D printing scaffold designs [33-35]. Also, hydrogel-based biomaterials are recently being investigated for soft tissue bio-printing applications. In recent years, bio-printing using hydrogels has been carried out to produce artificial tissues such as artificial ears [36], bones [34], vascular tissues [37], and cartilage structures[38]. In these studies, the artificial tissue is made in a 3D shape with living cells and biocompatible materials [39-41].

3D printing has received much attention recently due to its various advantages in tissue engineering [42, 43]. Studies using various materials have been continuing. Among them, there is a method of printing through a decellularized ECM [44]. It has been found that the hydrogels derived from natural biomaterials have superior biocompatibility and bioactivity compared to synthetic hydrogels [45]. Moreover, decellularized ECM has the advantage of being able to hydrogel with simple methods of controlling temperature and pH [46]. However, decellularized ECM in printing has a disadvantage in that it takes a relatively long time and has a poor physical property. Besides, there are no methods to control these characteristics [22]. We have studied to overcome these disadvantages and develop appropriate bio-inks.

We applied it to decellularized ECM concerning a previous study in which tyramine was modified in hyaluronic acid [47]. Decellularized ECM can also react with tyrosinase. Using this point, we used tyrosinase to induce conjugation between tyramine modified hyaluronic acid and decellularized ECM. In the end, modified bio-ink was developed by combining with hyaluronic acid to which tyramine was modified.

3.2 Materials and methods

3.2.1 Materials

Hyaluronic acid (40 – 64kDa) was purchased from Lifecore Biomedical, LLC (Chaska, MN). N-hydroxysuccinimide (NHS), 1-Ethyl-3-(3-dimethylaminopropyl) carbodiimide hydrochloride (EDC·HCL), Tyramine hydrochloride were all purchased from Sigma-Aldrich. The recombinant tyrosinases from Streptomyces avermitilis were expressed in Escherichia coli. All solutions were sterilized with mixed cellulose ester membrane which cut-off size is 0.22μm (Daihan Scientific, Korea).

3.2.2 Decellularization of porcine brain

The decellularization process was carried out using the porcine brain. The decellularization process proceeded with the method used in the previous study. Briefly, for decellularization, the frozen brain tissue was thawed in a 25° C water bath. Its dura mater was carefully removed and cut into small pieces of 1 x 1 x 1 cm3. Wash 3 times with DI water between all the processes mentioned below. The pieces

are placed in DI water and washed at 60 rpm 24 hours. Then We incubated for 120 minutes in 3% (v / v) Triton X-100(Sigma) with 0.1% (v / v) ammonium hydroxide (Sigma). Then, immerse in 1M sucrose solution for 30 minutes and 4% (Sigma) for 2 hours. The ECM obtained was incubated at room temperature for 12 hours using 2,000 Kunitz units DNase (Sigma, D4263). Finally, it is washed in PBS containing 1% (v/v) penicillin-streptomycin (Thermo Fisher Scientific) for 30 minutes and then lyophilized. The decellularized ECM (DECM) thus obtained is dissolved at a concentration of 15 mg/mL in a solution of 10 mg/mL of pepsin dissolved in 0.01 N HCl. After 48 hours, titrate pH to 7.4 and store at 4 ° C.

3.2.3 Synthesis of tyramine-modified hyaluronic acid(HA_T)

1.0 % (w/v) HA solution was prepared by dissolving 100 mg of sodium hyaluronate (Lifecore Biomedical, USA) in 10 mL of Deionized water. After completely dissolved, tyramine hydrochloride (Sigma-Aldrich, the molar ratio of tyramine/COOH in HA =1) was added to the solution. Under constant stirring, N-hydroxysulfosuccinimide (sulfo-NHS; Sigma-Aldrich, USA) and N-(3-dimethylaminopropyl)-N′-ethylcarbodiimide (EDC; Thermo Fisher Scientific) were added to the solution. The molar ratio of EDC: tyramine = 1: 1. The mixture was stirred for overnight to complete the reaction. The HA-Tyramine conjugate was purified by dialysis membrane (SnakeskinTM dialysis membrane; Thermo Fisher Scientific) against distilled water for 3 days, filtered, and lyophilized for storage. The final product was analyzed by NMR and UV-Vis spectrometer.

3.2.4 Preparation of hydrogels

The hydrogel was prepared using previously synthesized HA_T and DECM solution. First, HA-T 4% (w / v) was dissolved in deionized water. After completely dissolved, HA_T solutions were sterilized by the syringe-driven filtration (200 nm mesh). In HA-TD2%, it was prepared by uniformly mixing HA-T4% solution and 1% DECM at a ratio of 1: 1 and adding SA_Ty to a final concentration of 10 uM. HA_T1% and HA_T0.5% were prepared by adjusting the ratio of HA_T 4% solution in the same method. D hydrogel was prepared by uniformly mixing 1% deionized water and 1% DECM and then adding SA_Ty to a final concentration of 10 uM. The compositions of each hydrogel were summarized in Table.

3.2.5 Rheological analysis

Rheological analysis of hydrogel was conducted in Demo lab (Anton Paar Korea) using rheometer (MCR 302, Measuring cell: P-PTD & H-PTD 200, Measuring System: PP 25, Anton-Paar, Austria). All samples were 8 mm in diameter and 2 mm thick. All experiments were conducted at 37° C and air flow. Firstly, we performed a strain sweep test. It was conducted to evaluate critical strain. When the strain increases, the intersection point of G' and G" is the critical strain. Next, we performed the frequency sweep test. The G' and G" was measured when decreasing frequency from 100 Hz to 0.1 Hz. The strain was fixed at 3 %. Finally, a time sweep test was performed to measure the gelation time. G' and G" were measured for 10 min under constant conditions of 2 % strain.

3.2.6 Swelling ratios analysis

To proceed with the experiment, the hydrogel was prepared by the method described previously. For making a uniform shape, a 8 mm diameter frame made with PDMS was used. This mixture was incubated at 37 ° C for overnight to complete gelation. After hydrogel was made, it was transferred to Deionized water and swelled sufficiently at 37° C. The swelled hydrogel was frozen in a deep freezer after weighing and then lyophilized. The swelling ratio of hydrogel was measured by the following equations.

3.2.7 Scanning electron microscopy(SEM) analysis

We analyzed the internal structure of hydrogel using SEM. All hydrogel was prepared by the method described previously. All of the lyophilized samples were cut horizontally using a blade and mounted on SEM mounts with carbon tape. Before the measurement, the samples were coated with platinum/palladium for 120 seconds in vacuum. The image was observed by JSM-7610F Scanning Electron Microscope (JEOL USA, Inc.) at 10 μA and 10 kV.

3.2.8 Measurement of Young’s modulus

Young's modulus was measured by using a UTM. Briefly, we fabricated all samples of uniform shape using a PDMS mold with a diameter of 8mm and a height of 2 mm. Then, samples were pressed at a rate of 1 mm/min of probe speed using a UTM. The Young's modulus was calculated from a linear region of the stress-strain curve (5-15% strain).

3.2.9 Statistical analysis

All data are expressed as mean and standard deviation (SD). Statistical significance was evaluated by Student's t-test with *P < 0.05, **P < 0.01, or *** < 0.001

3.3 Results & Discussion

3.3.1 Synthesis and characterization of decellularized ECM-based hydrogel

First, we confirmed that the decellularization process was successful. When the sample before and after the decellularization process was examined by H&E, it was confirmed that no cells were observed in the sample after the process. (Fig. 3.3 A) DNA content was then measured by the picogreen assay, which contained 38.92 ng/mg. (Fig. 3.3 B) It was about 96% less than before decellularization. Finally, there was no difference in the loss of GAGs when comparing before and after decellularization. (Fig. 3.3 C) The tilting test confirmed that decellularized ECM-based hydrogel required 15 minutes to 30 minutes to complete at 37 ° C. (Fig. 3.4)

3.3.2 Mechanical and physical properties of hydrogels

Next, we investigated the initial behavior of gelation through rheological analysis. When the time sweep test was performed using only HA_T2%, it was confirmed that the hydrogel was stabilized in about 10 minutes. (Fig. 3.5 A.a) Afterward, gelation was carried out by mixing HA_T with decellularized ECM of the final concentration of 0.5%. (Fig. 3.5 A.b-d) It was stabilized at a fast rate as compared with the previous one, and the higher the concentration of HA_T, the faster the saturation was. To confirm that the decellularized ECM is gelated by the temperature, a time sweep test was conducted with the temperature linearly increasing from 4 to 37 degrees. The results were confirmed to be gelation with the term considering the time difference of the temperature of the equipment to be transferred to the hydrogel. (Fig. 3.5 A.e)

Frequency sweep test and shear strain test were then performed. From these results, it was confirmed that the higher the concentration of HA_T, the higher the physical properties and the stable physical properties at 1 ~ 10Hz. (Fig. B, C) Young's modulus was measured through UTM equipment. Similar to the previous data, it can be seen that Young's modulus increases as HA_T concentration mixed with decellularized ECM increases. (Fig. 3.6 A) Then, it was confirmed that the higher the HA_T concentration, the lower the swelling ratio. (Fig. 3.6 B) These results suggest that the binding between HA-T and decellularized ECM reinforces the lack of physical properties. In the SEM image, collagen fiber structure was observed in all hydrogel containing decellularized ECM. (Fig. 3.7)

3.3.3 Further work

We have developed a hydrogel that can overcome the disadvantages of decellularized ECM. These hydrogels have the potential to be used in various places through injectable properties. In particular, we confirmed the possibility of producing various scaffolds by applying to 3D printing. Decellularized ECM is thought to be a bio-link with more utility value if it is used together with biocompatible materials such as alginate or gelatin.

REFERENCES

[1] L.G. Griffith, G.J.s. Naughton, Tissue engineering--current challenges and expanding opportunities, 295(5557) (2002) 1009-1014.
[2] A.I.J.J.o.c.p. Caplan, Adult mesenchymal stem cells for tissue engineering versus regenerative medicine, 213(2) (2007) 341-347.
[3] P.M. Bartold, C.A. Mcculloch, A.S. Narayanan, S.J.P. Pitaru, Tissue engineering: a new paradigm for periodontal regeneration based on molecular and cell biology, 24(1) (2000) 253-269.
[4] A. Usas, J.J.B. Huard, Muscle-derived stem cells for tissue engineering and regenerative therapy, 28(36) (2007) 5401-5406.
[5] A. Chilkoti, T. Christensen, J.A.J.C.o.i.c.b. MacKay, Stimulus responsive elastin biopolymers: applications in medicine and biotechnology, 10(6) (2006) 652-657.
[6] J. Zhuang, M.R. Gordon, J. Ventura, L. Li, S.J.C.S.R. Thayumanavan, Multi-stimuli responsive macromolecules and their assemblies, 42(17) (2013) 7421-7435.
[7] J.F.J.A.E.M. Mano, Stimuli-responsive polymeric systems for biomedical applications, 10(6) (2008) 515-527.
[8] N. Tandon, C. Cannizzaro, P.-H.G. Chao, R. Maidhof, A. Marsano, H.T.H. Au, M. Radisic, G.J.N.p. Vunjak-Novakovic, Electrical stimulation systems for cardiac tissue engineering, 4(2) (2009) 155.
[9] K.Y. Lee, M.C. Peters, K.W. Anderson, D.J.J.N. Mooney, Controlled growth factor release from synthetic extracellular matrices, 408(6815) (2000) 998.
[10] A.S. Hoffman, P.S.J.P.i.P.S. Stayton, Conjugates of stimuli-responsive polymers and proteins, 32(8-9) (2007) 922-932.
[11] A.S.J.A.d.d.r. Hoffman, Hydrogels for biomedical applications, 64 (2012) 18-23.
[12] S. Yang, K.-F. Leong, Z. Du, C.-K.J.T.e. Chua, The design of scaffolds for use in tissue engineering. Part I. Traditional factors, 7(6) (2001) 679-689.
[13] J.V. Higdon, B. Frei, Tea catechins and polyphenols: health effects, metabolism, and antioxidant functions, (2003).
[14] J.A. Nichols, S.K.J.A.o.d.r. Katiyar, Skin photoprotection by natural polyphenols: anti-inflammatory, antioxidant and DNA repair mechanisms, 302(2) (2010) 71-83.
[15] S. Valcic, A. Muders, N.E. Jacobsen, D.C. Liebler, B.N.J.C.r.i.t. Timmermann, Antioxidant chemistry of green tea catechins. Identification of products of the reaction of (−)-epigallocatechin gallate with peroxyl radicals, 12(4) (1999) 382-386.
[16] W.E. Hennink, C.F. van Nostrum, Novel crosslinking methods to design hydrogels, Advanced Drug Delivery Reviews 64 (2012) 223-236.
[17] L.S.M. Teixeira, J. Feijen, C.A. van Blitterswijk, P.J. Dijkstra, M.J.B. Karperien, Enzyme-catalyzed crosslinkable hydrogels: emerging strategies for tissue engineering, 33(5) (2012) 1281-1290.
[18] S.H. Lee, K. Baek, J.E. Lee, B.G.J.B. Kim, bioengineering, Using tyrosinase as a monophenol monooxygenase: A combined strategy for

effective inhibition of melanin formation, 113(4) (2016) 735-743.
[19] T.W. Gilbert, T.L. Sellaro, S.F.J.B. Badylak, Decellularization of tissues and organs, 27(19) (2006) 3675-3683.
[20] S.F. Badylak, D.O. Freytes, T.W. Gilbert, Extracellular matrix as a biological scaffold material: Structure and function, Acta Biomaterialia 5(1) (2009) 1-13.
[21] P.M. Crapo, T.W. Gilbert, S.F.J.B. Badylak, An overview of tissue and whole organ decellularization processes, 32(12) (2011) 3233-3243.
[22] M.T. Wolf, K.A. Daly, E.P. Brennan-Pierce, S.A. Johnson, C.A. Carruthers, A. D'Amore, S.P. Nagarkar, S.S. Velankar, S.F.J.B. Badylak, A hydrogel derived from decellularized dermal extracellular matrix, 33(29) (2012) 7028-7038.
[23] D.A. Young, D.O. Ibrahim, D. Hu, K.L.J.A.b. Christman, Injectable hydrogel scaffold from decellularized human lipoaspirate, 7(3) (2011) 1040-1049.
[24] B. Sharma, S. Fermanian, M. Gibson, S. Unterman, D.A. Herzka, B. Cascio, J. Coburn, A.Y. Hui, N. Marcus, G.E.J.S.t.m. Gold, Human cartilage repair with a photoreactive adhesive-hydrogel composite, 5(167) (2013) 167ra6-167ra6.
[25] J. Elisseeff, A. Ferran, S. Hwang, S. Varghese, Z.J.S.c. Zhang, development, The role of biomaterials in stem cell differentiation: applications in the musculoskeletal system, 15(3) (2006) 295-303.
[26] S.B. Seif-Naraghi, D. Horn, P.J. Schup-Magoffin, K.L. Christman, Injectable extracellular matrix derived hydrogel provides a platform for enhanced retention and delivery of a heparin-binding growth factor, Acta Biomaterialia 8(10) (2012) 3695-3703.
[27] F. Pati, J. Jang, D.-H. Ha, S.W. Kim, J.-W. Rhie, J.-H. Shim, D.-H. Kim, D.-W.J.N.c. Cho, Printing three-dimensional tissue analogues with decellularized extracellular matrix bioink, 5 (2014) 3935.
[28] T. Boland, T. Xu, B. Damon, X.J.B.J.H.N.T. Cui, Application of inkjet printing to tissue engineering, 1(9) (2006) 910-917.
[29] S.C. Cox, J.A. Thornby, G.J. Gibbons, M.A. Williams, K.K.J.M.S. Mallick, E. C, 3D printing of porous hydroxyapatite scaffolds intended for use in bone tissue engineering applications, 47 (2015) 237-247.
[30] K. Markstedt, A. Mantas, I. Tournier, H.c. Martı´nez A´vila, D. Ha¨gg, P.J.B. Gatenholm, 3D bioprinting human chondrocytes with nanocellulose-alginate bioink for cartilage tissue engineering applications, 16(5) (2015) 1489-1496.
[31] V. Mironov, T. Boland, T. Trusk, G. Forgacs, R.R.J.T.i.B. Markwald, Organ printing: computer-aided jet-based 3D tissue engineering, 21(4) (2003) 157-161.
[32] V. Mironov, N. Reis, B.J.T.e. Derby, Bioprinting: A beginning, 12(4) (2006) 631-634.
[33] H. Seitz, W. Rieder, S. Irsen, B. Leukers, C. Tille, Three-dimensional printing of porous ceramic scaffolds for bone tissue engineering, J. Biomed. Mater. Res. Part B 74B(2) (2005) 782-788.
[34] S. Bose, S. Vahabzadeh, A. Bandyopadhyay, Bone tissue engineering using 3D printing, Materials Today 16(12) (2013) 496-504.
[35] A. Khalyfa, S. Vogt, J. Weisser, G. Grimm, A. Rechtenbach, W. Meyer,

M. Schnabelrauch, Development of a new calcium phosphate powder-binder system for the 3D printing of patient specific implants, J. Mater. Sci.-Mater. Med. 18(5) (2007) 909-916.
[36] M.S. Mannoor, Z. Jiang, T. James, Y.L. Kong, K.A. Malatesta, W.O. Soboyejo, N. Verma, D.H. Gracias, M.C. McAlpine, 3D Printed Bionic Ears, Nano Letters 13(6) (2013) 2634-2639.
[37] C. Norotte, F.S. Marga, L.E. Niklason, G. Forgacs, Scaffold-free vascular tissue engineering using bioprinting, Biomaterials 30(30) (2009) 5910-5917.
[38] S. Mayer-Wagner, T.S. Schiergens, B. Sievers, J.I. Redeker, B. Schmitt, A. Buettner, V. Jansson, P.E. Müller, Scaffold-free 3D cellulose acetate membrane-based cultures form large cartilaginous constructs, Journal of Tissue Engineering and Regenerative Medicine 5(2) (2011) 151-155.
[39] S.V. Murphy, A. Atala, 3D bioprinting of tissues and organs, Nature biotechnology 32(8) (2014) 773.
[40] H.-W. Kang, S.J. Lee, I.K. Ko, C. Kengla, J.J. Yoo, A.J.N.b. Atala, A 3D bioprinting system to produce human-scale tissue constructs with structural integrity, 34(3) (2016) 312.
[41] M. Nakamura, A. Kobayashi, F. Takagi, A. Watanabe, Y. Hiruma, K. Ohuchi, Y. Iwasaki, M. Horie, I. Morita, S.J.T.e. Takatani, Biocompatible inkjet printing technique for designed seeding of individual living cells, 11(11-12) (2005) 1658-1666.
[42] H.N. Chia, B.M.J.J.o.b.e. Wu, Recent advances in 3D printing of biomaterials, 9(1) (2015) 4.
[43] W. Zhu, X. Ma, M. Gou, D. Mei, K. Zhang, S.J.C.o.i.b. Chen, 3D printing of functional biomaterials for tissue engineering, 40 (2016) 103-112.
[44] J. Jang, H.-J. Park, S.-W. Kim, H. Kim, J.Y. Park, S.J. Na, H.J. Kim, M.N. Park, S.H. Choi, S.H.J.B. Park, 3D printed complex tissue construct using stem cell-laden decellularized extracellular matrix bioinks for cardiac repair, 112 (2017) 264-274.
[45] M.T. Wolf, K.A. Daly, E.P. Brennan-Pierce, S.A. Johnson, C.A. Carruthers, A. D'Amore, S.P. Nagarkar, S.S. Velankar, S.F. Badylak, A hydrogel derived from decellularized dermal extracellular matrix, Biomaterials 33(29) (2012) 7028-7038.
[46] M.J. Sawkins, W. Bowen, P. Dhadda, H. Markides, L.E. Sidney, A.J. Taylor, F. Rose, S.F. Badylak, K.M. Shakeshehh, L.J. White, Hydrogels derived from demineralized and decellularized bone extracellular matrix, Acta Biomaterialia 9(8) (2013) 7865-7873.
[47] S.-H. Kim, S.-H. Lee, J.-E. Lee, S.J. Park, K. Kim, I.S. Kim, Y.-S. Lee, N.S. Hwang, B.-G. Kim, Tissue adhesive, rapid forming, and sprayable ECM hydrogel via recombinant tyrosinase crosslinking, Biomaterials 178 (2018) 401-412.

초록(국문요약)

최근 조직공학 분야에서 다양한 재료에 기능성을 부여하는 시도들이 계속되고 있다. 특히 주사 가능한 하이드로겔은 상처 부위를 최소화할 수 있는 장점을 가지고 있어 꾸준히 연구되어 왔는데, 최근 들어 3D-프린팅 재료로서 사용될 수 있는 가능성 때문에 또다시 주목받고 있다. 우리는 녹차추출물인 Epigallocatechin gallate(EGCG)와 같은 기능성 분자 또는 다양한 생체신호 물질을 포함한 탈세포된 세포 외 기질을 이용해 주사 가능한 하이드로겔을 개발했다. Streptomyces avermitilis(SA_Ty)를 통해 EGCG를 산화시켜 제작한 키토산 기반 하이드로겔은 항 염증 능력을 가진다. 또한 상처 회복 모델을 통해 하이드로겔이 가지는 라디칼 소거 기능 때문에 면역반응이 조절되는 것을 확인했다. 또한 우리는 탈세포된 세포 외 기질과 Tyramine이 결합된 히알루론산을 적절히 배합하여 빠르게 가교 가능한 하이드로겔을 제작하였다. 종합하자면 우리가 제작한 하이드로겔은 상처 재생과 같은 질병에 효과적인 치료 효과를 보일 뿐 아니라 3D 프린팅 재료로서 사용 가능한 재료이다.

LIST OF FIGURES AND TABLE

Figures

Figure 2.1 Three main component of tissue engineering

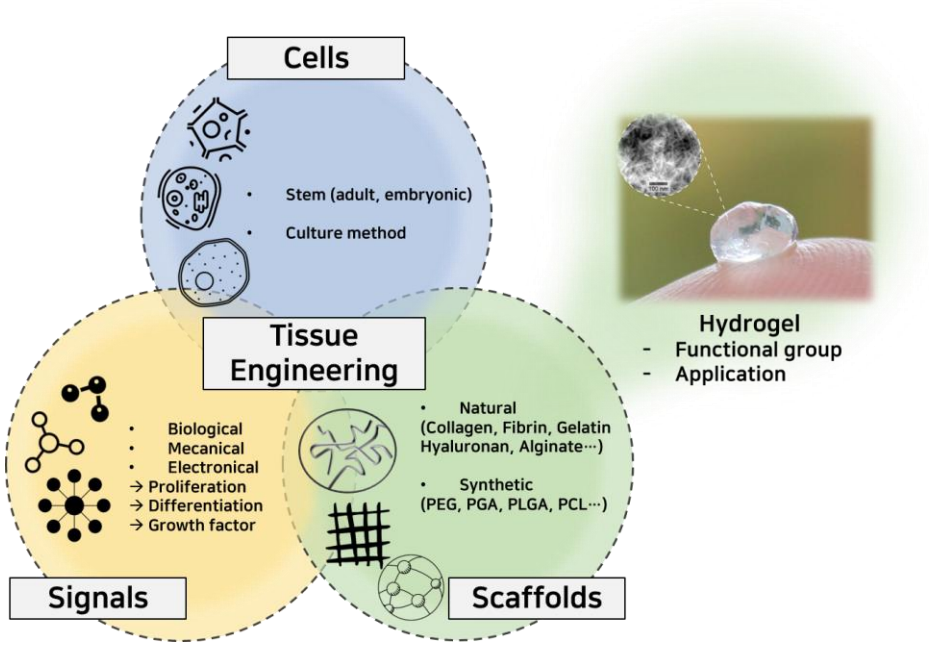

Figure 1.1 Three main component of tissue engineering

Figure 2.2 The overall scheme of polyphenol-functionalized chitosan hydrogels formed via an enzyme reaction

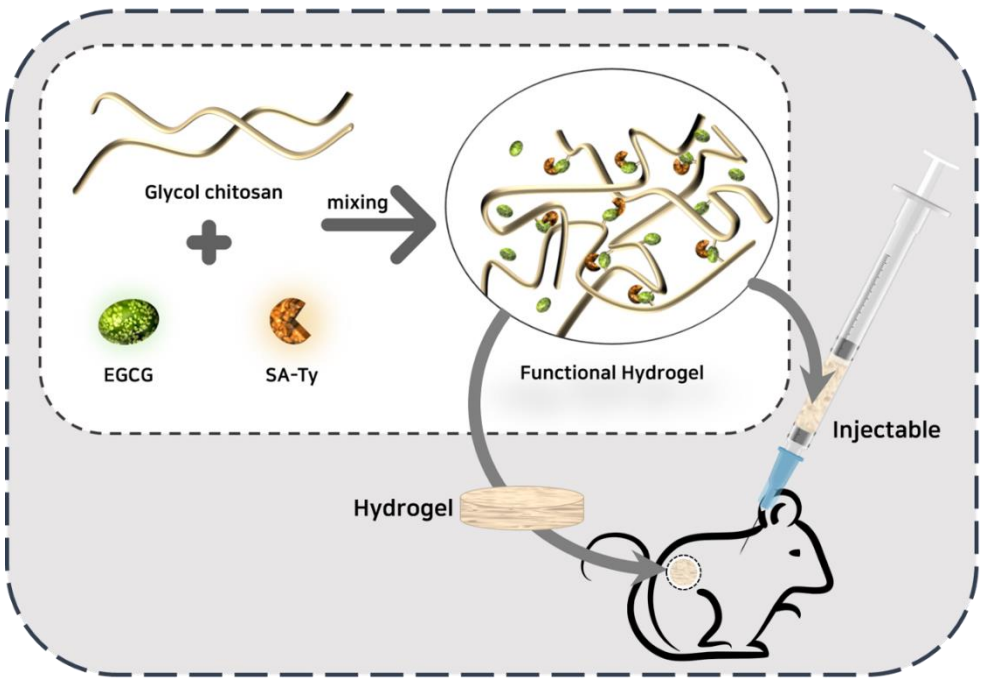

Figure 2.1. Schematic illustration of forming polyphenol-functionalized chitosan hydrogel

Figure 2.3 Mechanism of Chitosan-E hydrogels

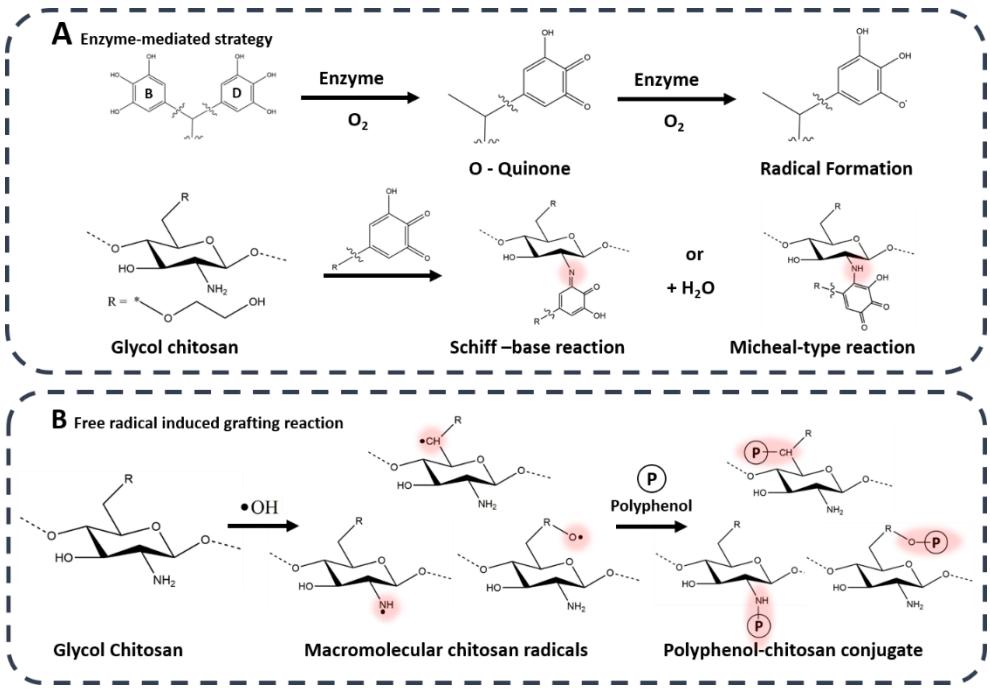

Figure 2.2. Two gelation mechanisms using enzymes. (A) Enzyme-mediated strategy. (B) Free radical-induced grafting reaction.

Figure 2.4 Sol fraction of Chitosan-E hydrogels

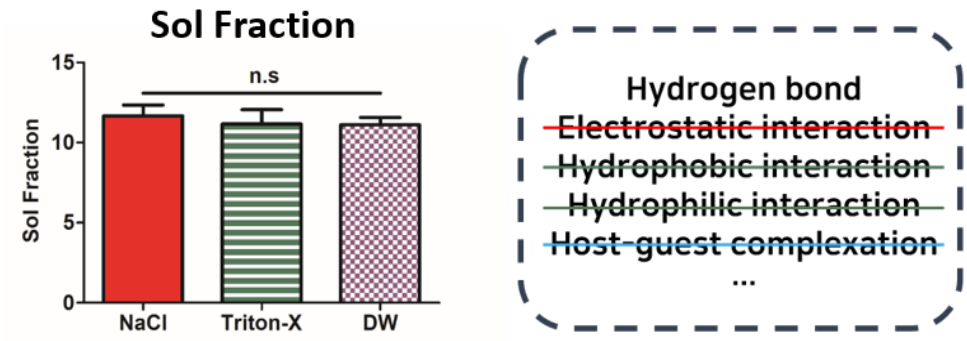

Figure 2.3. Sol fraction to determine the main binding of hydrogels

Figure 2.5 Gelation of Chitosan-E hydrogels

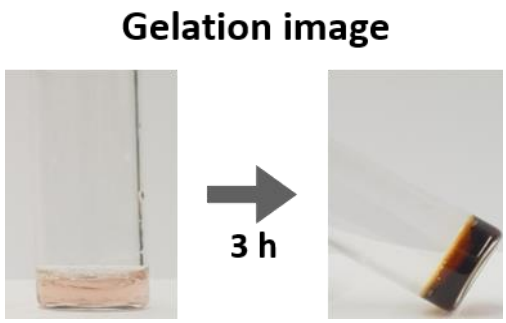

Figure 2.4. Gelation images of Chitosan-E hydrogel

Figure 2.6 Rheological analysis of Chitosan-E hydrogels

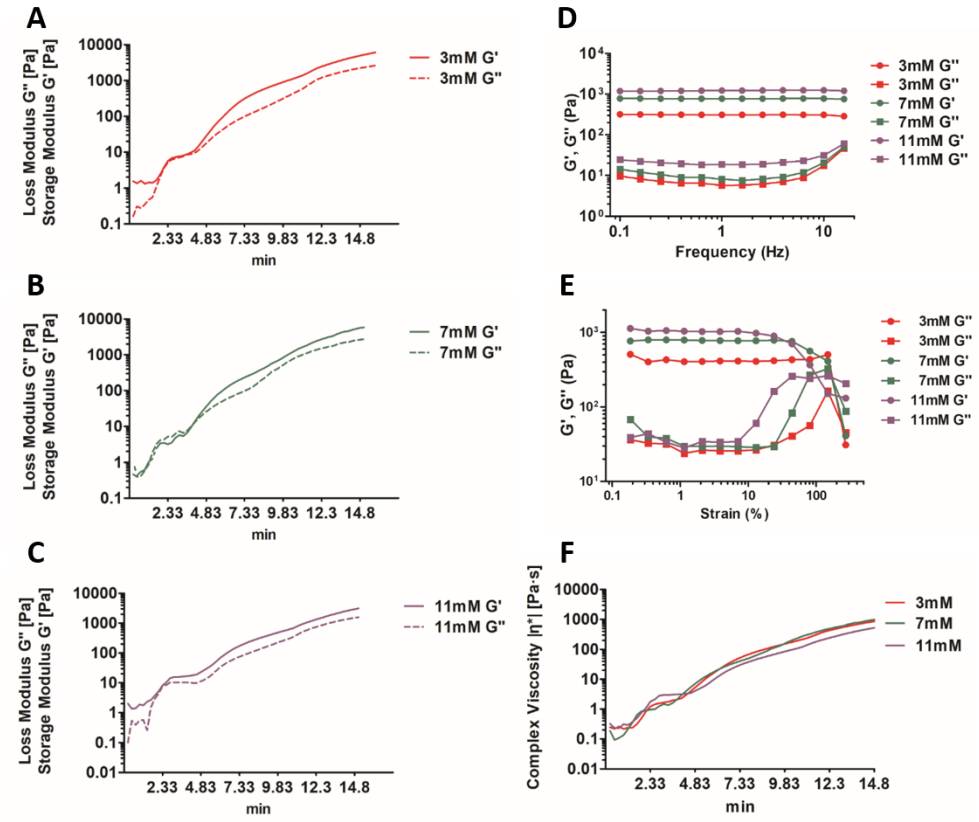

Figure 2.4. Rheological analysis of Chitosan-E hydrogels. (A-C) Time sweep test of 3mM, 7mM, and 11mM to determine gelation time. (D) Frequency sweep test of Chitosan- EGCG hydrogel. (E) Shear strain test of the hydrogel. (F) Complex viscosity of hydrogel. G'=storage modulus. G''=Loss modulus.

Figure 2.7 Mechanical properties of Chitosan-E hydrogels

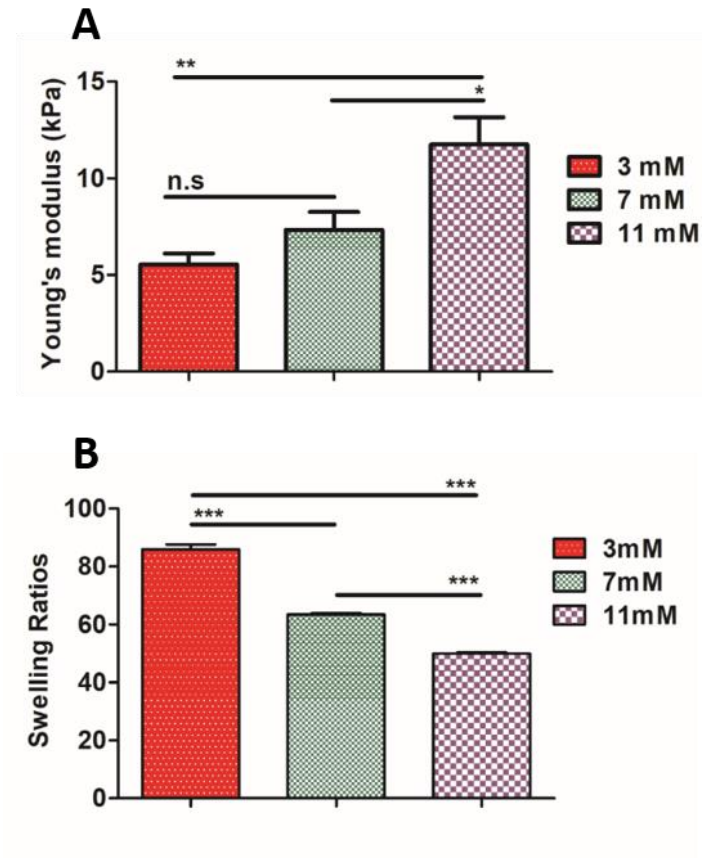

Figure 2.6. Mechanical properties of Chitosan-E hydrogels. (A) Young's modulus of Chitosan-E hydrogels (n=3). (B) Swelling ratios of Chitosan-E hydrogels (n=3)

Figure 2.8 Microstructure of Chitosan-E hydrogels

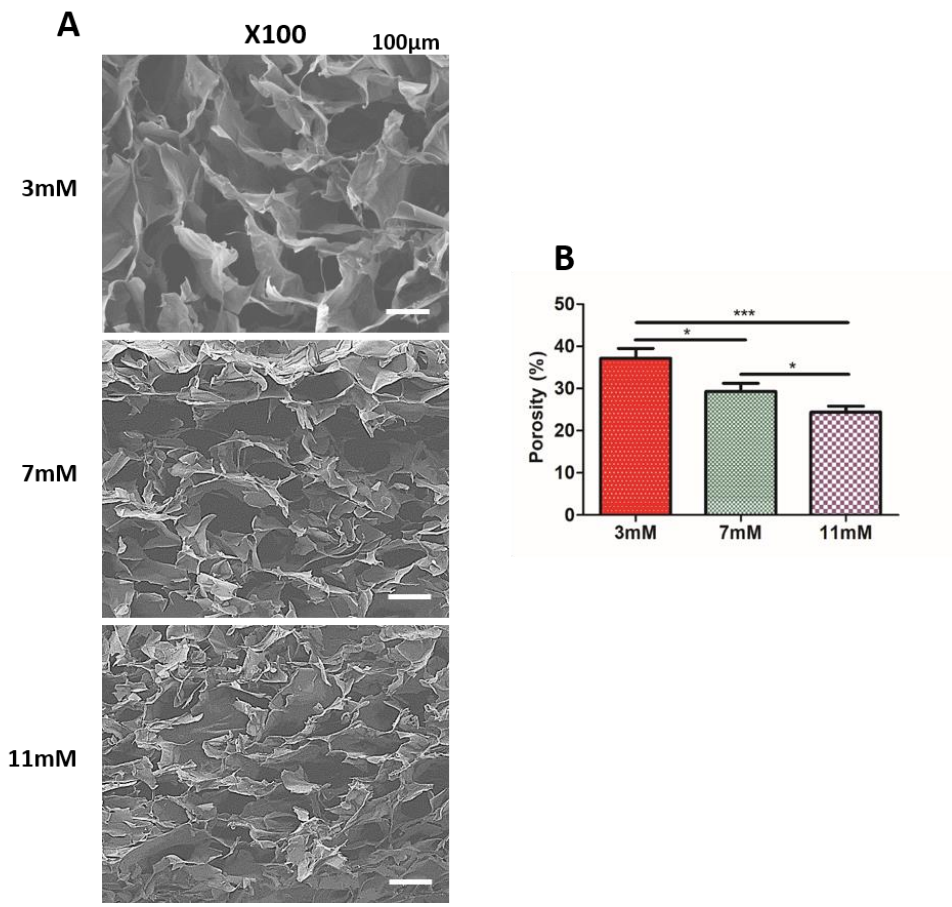

Figure 2.7. The microstructure of Chitosan-E hydrogels (A) Scanning electron microscope image. Scale bar=100μm. (B) The porosity of hydrogel. (n=3)

Figure 2.9 Releasing profile and function of hydrogel

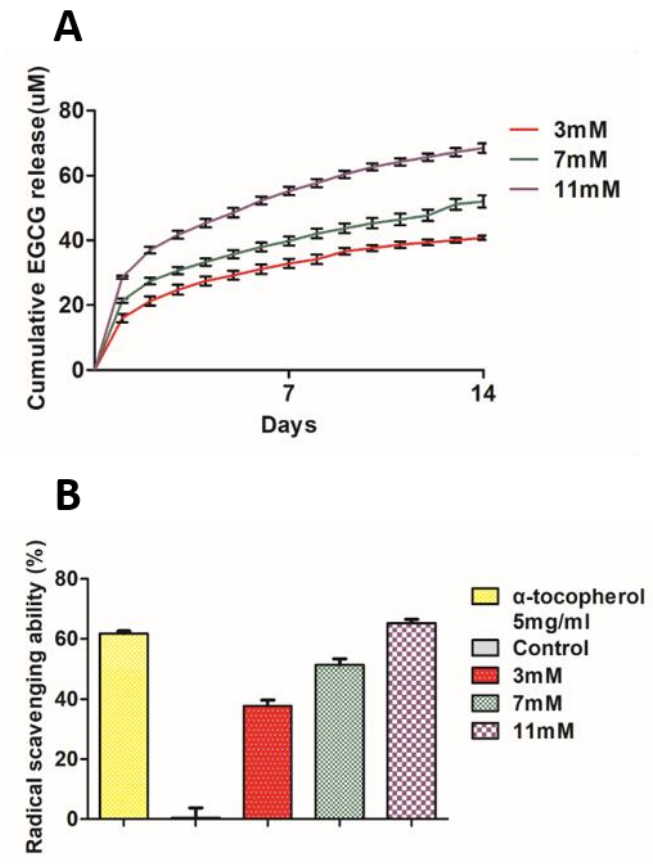

Figure 2.8. Releasing profile and function of Chitosan-E hydrogels. (A) EGCG releasing test of Chitosan-E hydrogels. (n=3) (B) Radical scavenging ability of hydrogel was measured by DPPH assay. (n=3)

Figure 2.10 Scheme of anti-bacterial test

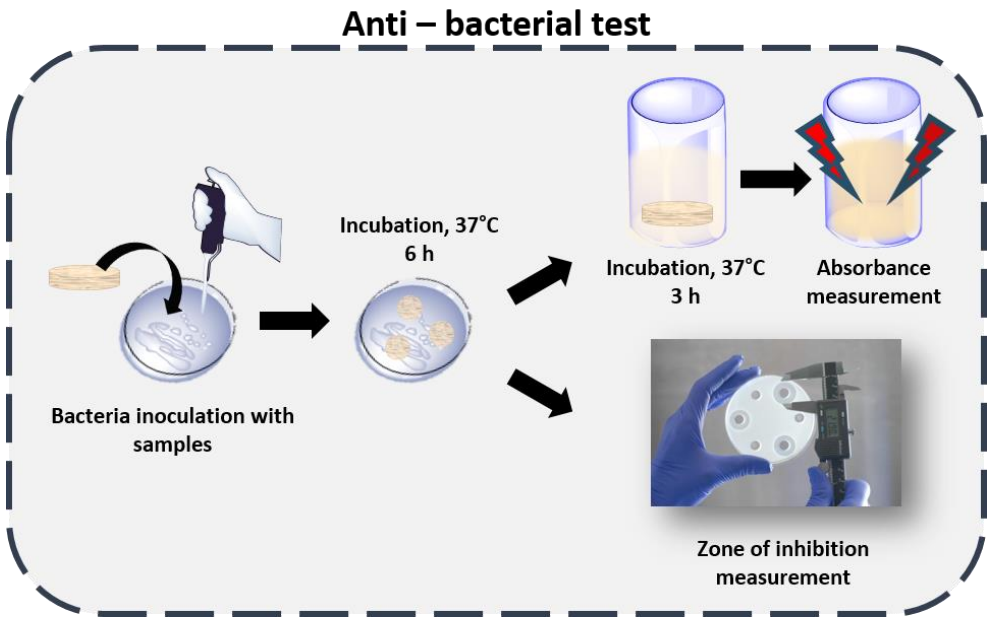

Figure 2.9. Schematic illustration of evaluating the hydrogel anti-bacterial ability.

Figure 2.11 Anti-bacterial ability of hydrogel

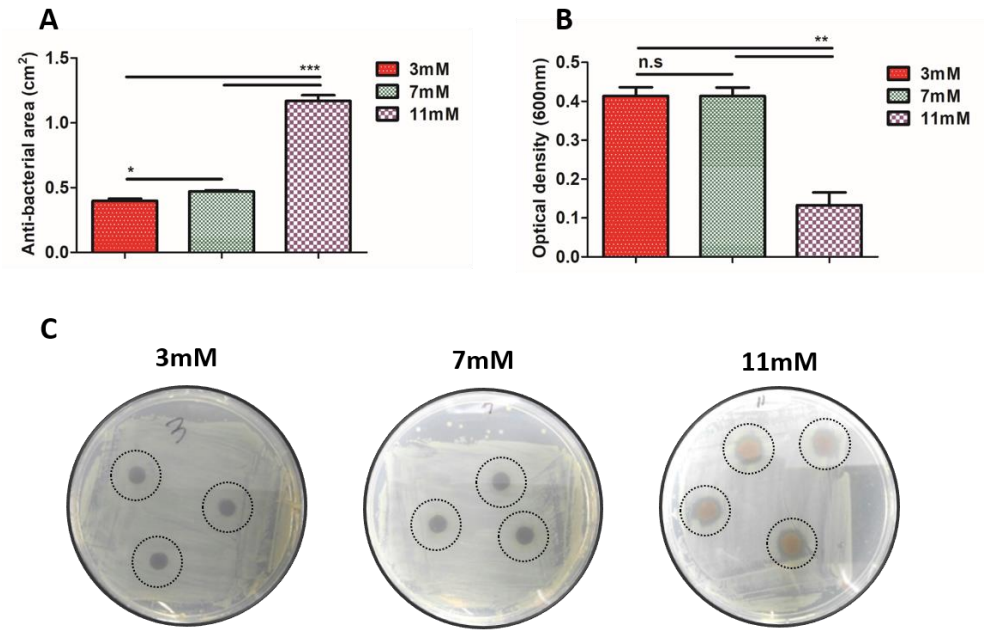

Figure 2.10. Anti-bacterial test. (A) Anti-bacterial ability was measured by calculating the inhibition area. (n=3) (B) Anti-bacterial ability was measured by optical density(600nm) after incubating the hydrogel in the medium. (n=3) (C) Inhibition zone images

Figure 2.12 Biocompatibility of hydrogel

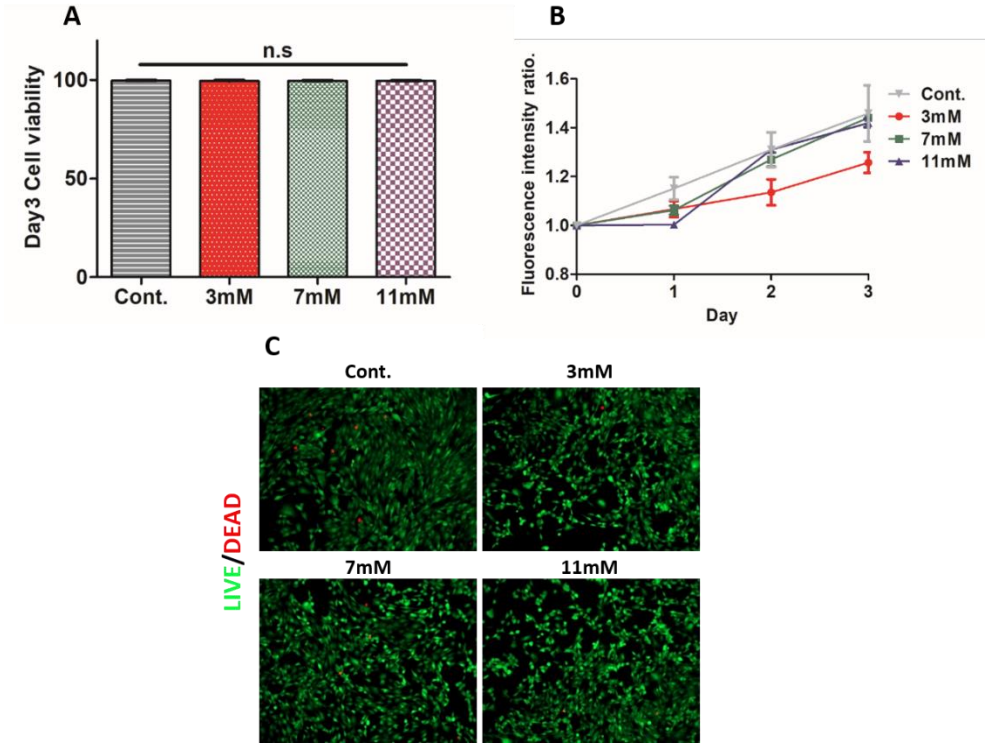

Figure 2.11. Biocompatibility of Chitosan-E hydrogels. (A) Live/Dead assay for dose-dependent EGCG. (n=3) (B) Cell viability was measured by PrestoBlue™ reagent. (n=3) (C) Live/Dead assay images; Live cell was stained with by Calcein AM (Green), and the dead cell was stained with by ethidium homodimer-1 (Red). (n=3)

Figure 2.13 Inflammation modulation ability of hydrogel

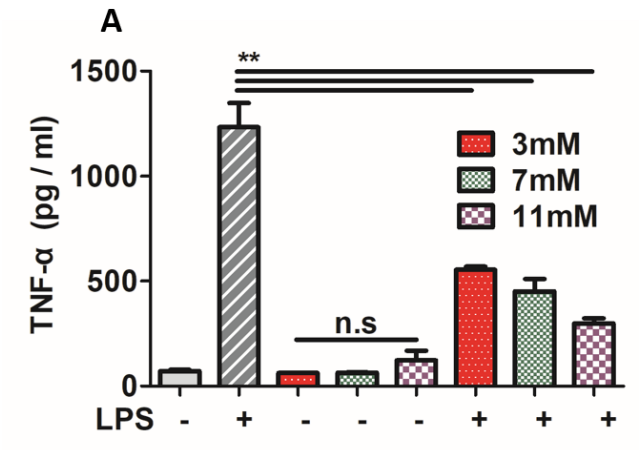

Figure 2.12. Inflammation modulation ability of hydrogel was measured by quantifying the amount of tissue necrosis factor alpha(TNF-α) from RAW 264.7 cells

Figure 2.14 Chitosan-E hydrogels injection model

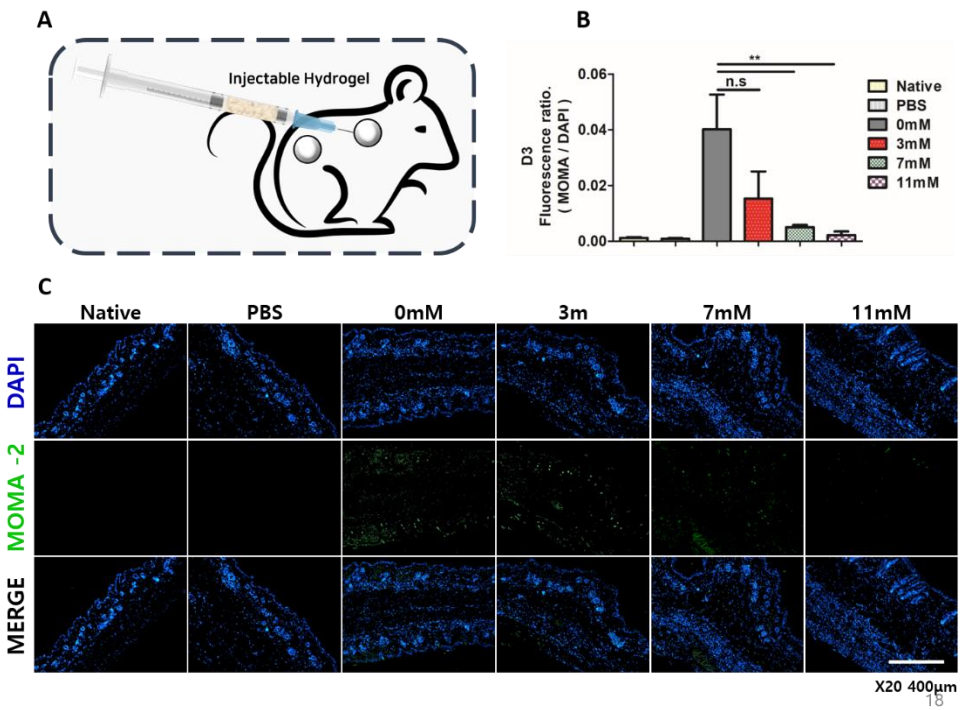

Figure 2.13. Chitosan-E hydrogels injection model to verifying the anti-inflammation ability of hydrogel. (A) Schematic illustration of the injection model. (B) The ratio of MOMA and DAPI calculated from the fluorescence ratio. (n=3). (C) Histological analysis of DAPI and Immunohistochemistry of MOMA-2 on day 3. Scale bar=400μm

Figure 2.15 Scheme of wound healing model and wound healing process

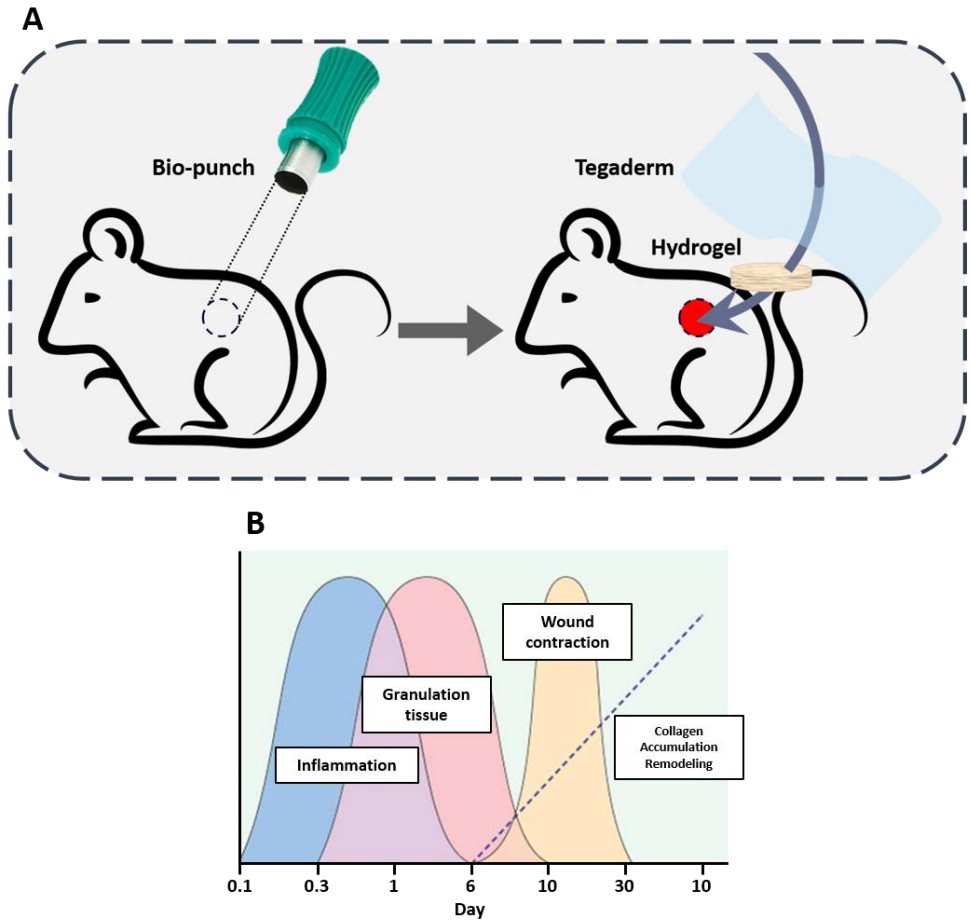

Figure 2.14. (A) Schematic illustration of wound healing model. (B) wound healing process graph.

Figure 2.16 Wound closing images and ratio

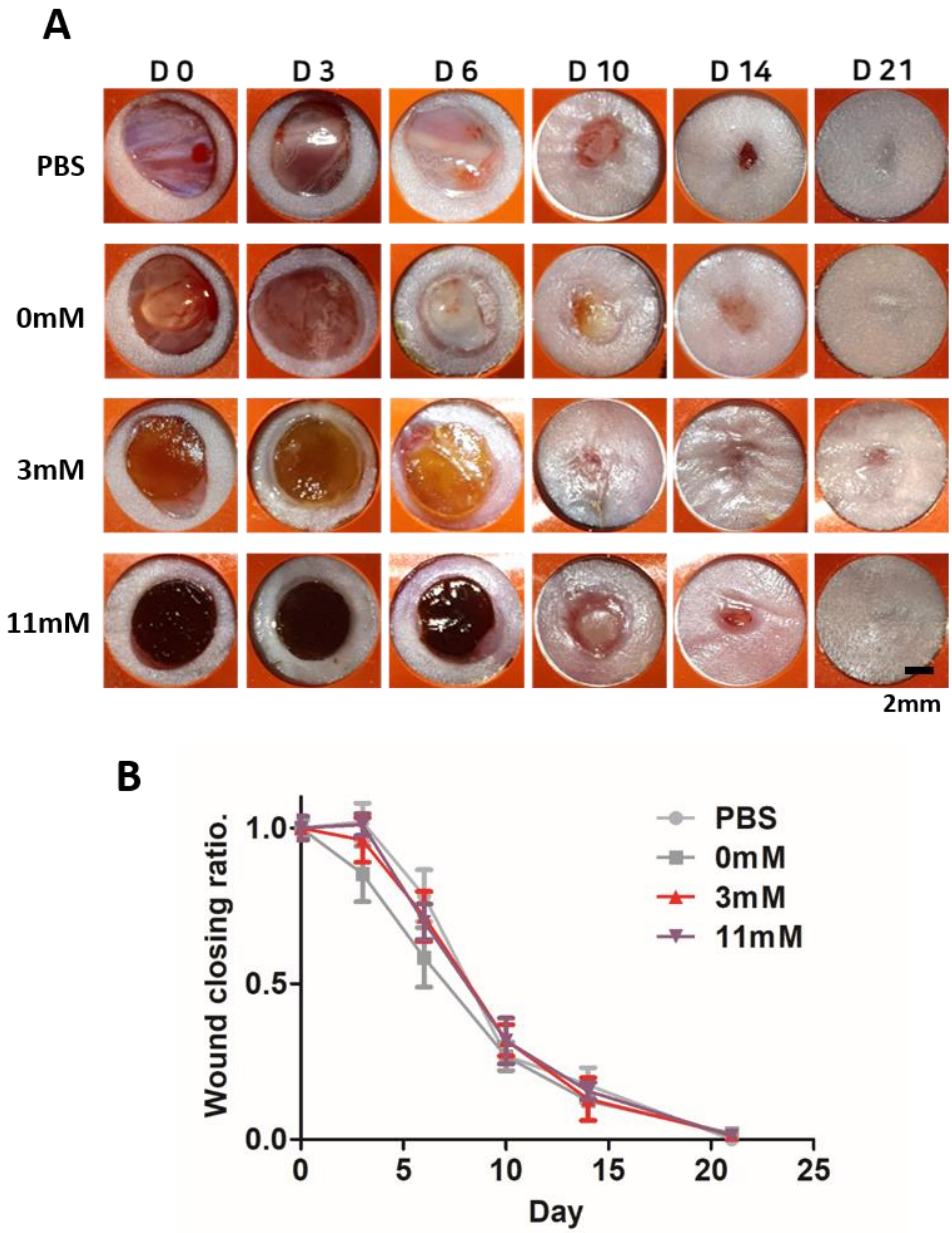

Figure 2.15. Wound healing model. (A) 0, 3, 6, 10, 14 and 21 days wound closing images. (B) Wound closing area ratio normalized to 0 day

Figure 2.17 Histology images

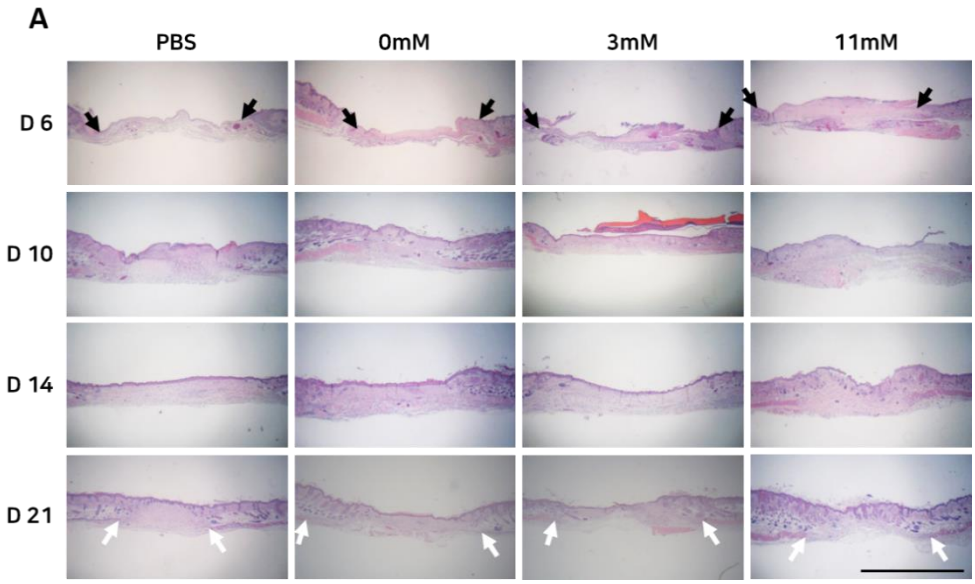

Figure 2.16. Hematoxylin and eosin histological analysis of wound healing. (A) Histological analysis of H&E at day 6, 10, 14 and 21. Scale bar=2mm. Black arrows highlight the epithelial tongue and white arrows point to the end of the panniculus carnosus (PC) muscle.

Figure 2.18 Immunohistochemistry of wound healing model

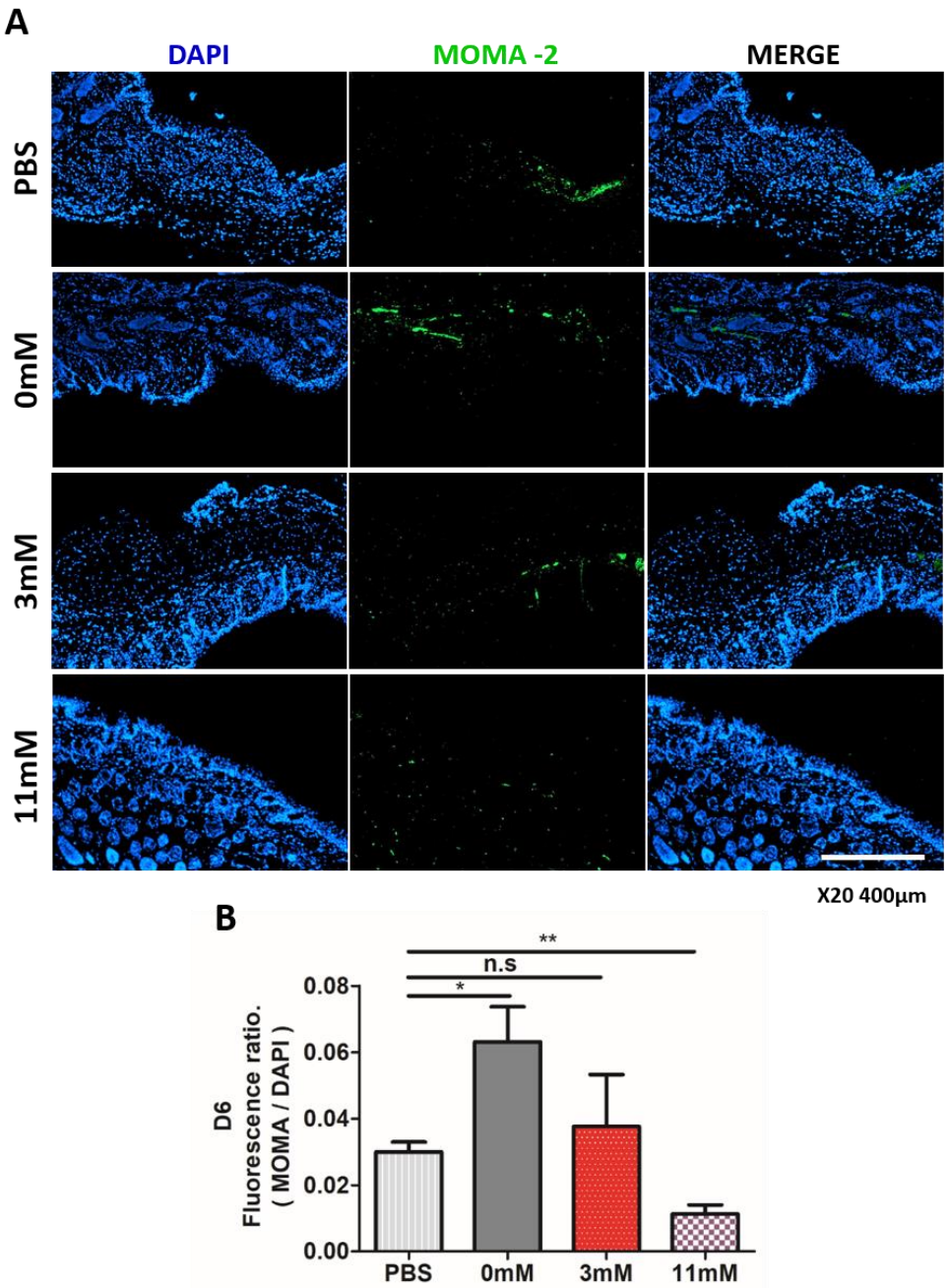

Figure 2.17. Immunohistochemistry of wound healing model. (A) Histological analysis of DAPI and Immunohistochemistry of MOMA-2 on day 3. Scale bar=400μm (B) The ratio of MOMA and DAPI calculated from the fluorescence ratio. (n=3).

Figure 2.19 *In vivo*, vascularization in the wound area

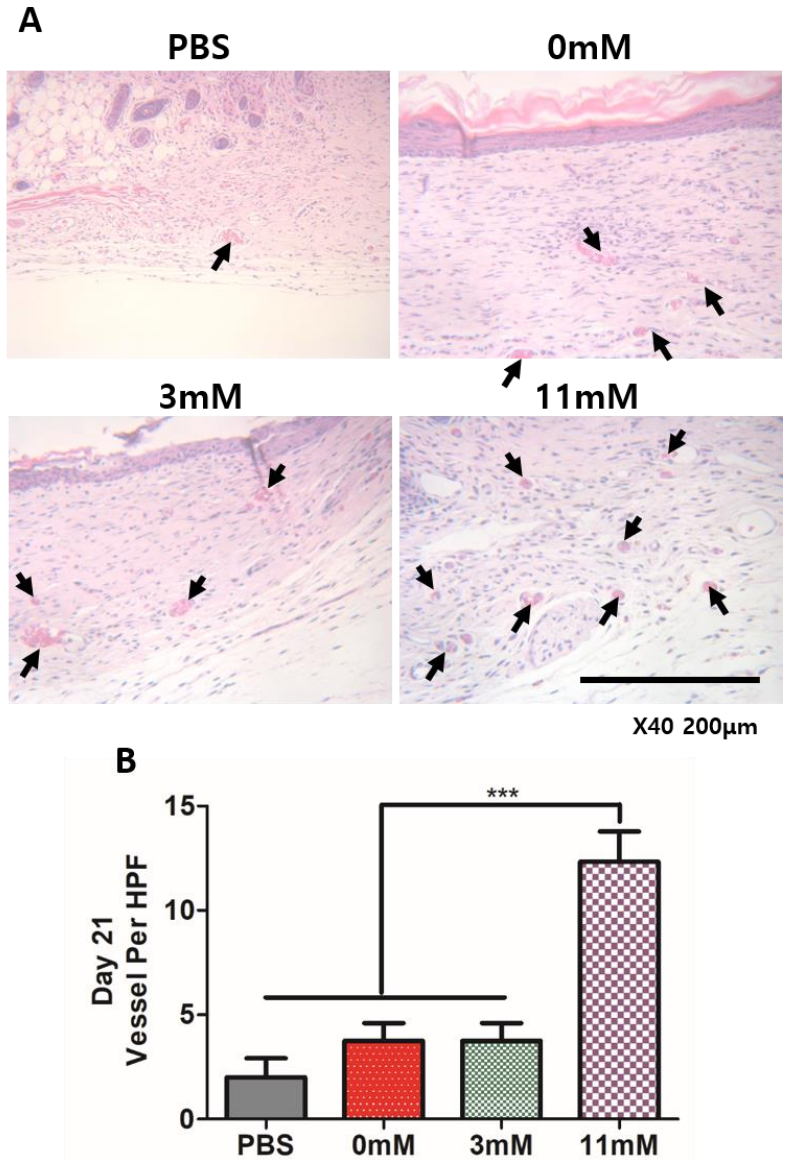

Figure 2.18. Measuring vascularization in the wound area. (A) High power field (HPF) (40X) imaging of the wound area. Scale bar=200µm Arrows highlight some of the vessels visible in H&E staining. (B) Number of vessels per HPF, n=3

Figure 3.1 Scheme for the synthesis of decellularized ECM-based hydrogel

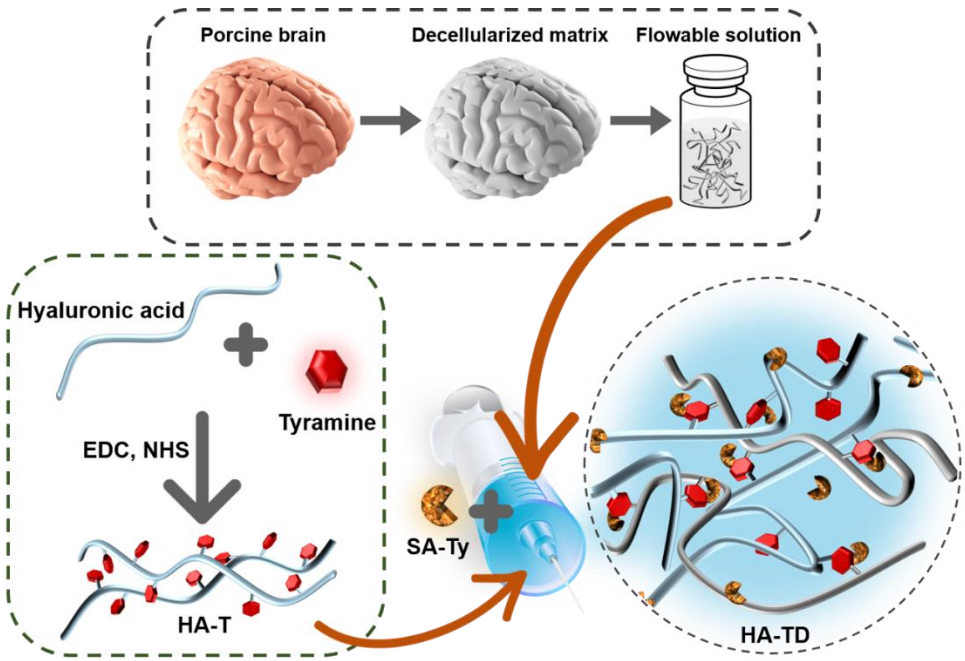

Figure 3.1. Schematic illustration of decellularized ECM-based hydrogel.

Figure 3.2 Decellularization step

Figure 3.2. Images of decellularization step.

Figure 3.3 Characterization of decellularized ECM

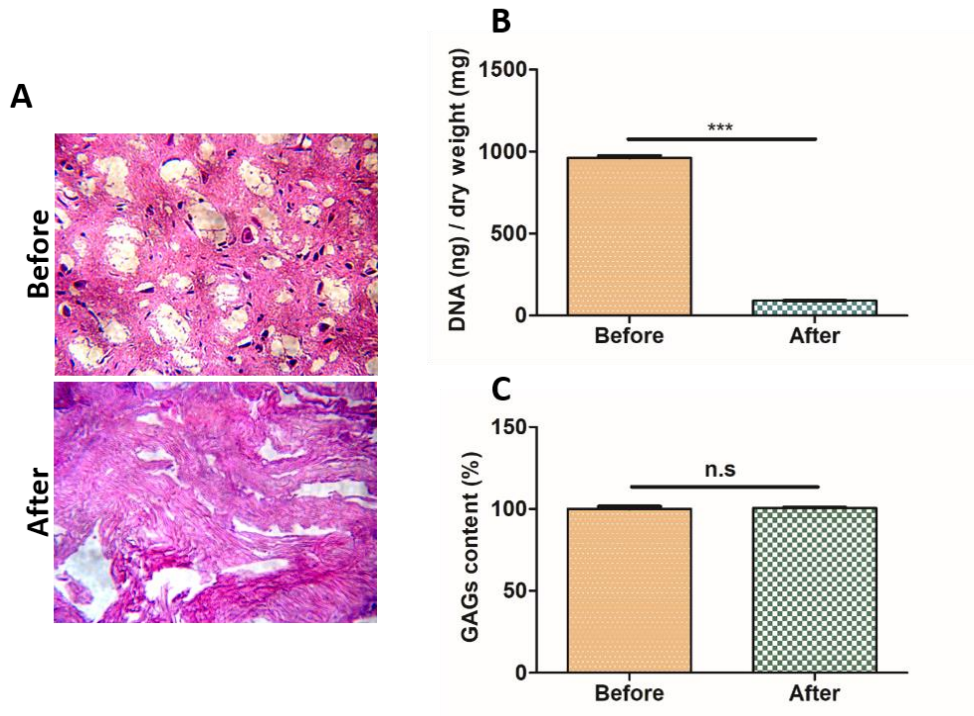

Figure 3.3. Characterization of decellularized ECM. (A) Histological analysis of H&E of before and after decellularization process. (B) Quantification of DNA content (DNA (ng)/dry weight (mg)) before and after the decellularization process. (n=5) (C) The ratio of GAGs content before and after the decellularization process. (n=5)

Figure 3.4 Gelation images of decellularized ECM hydrogel

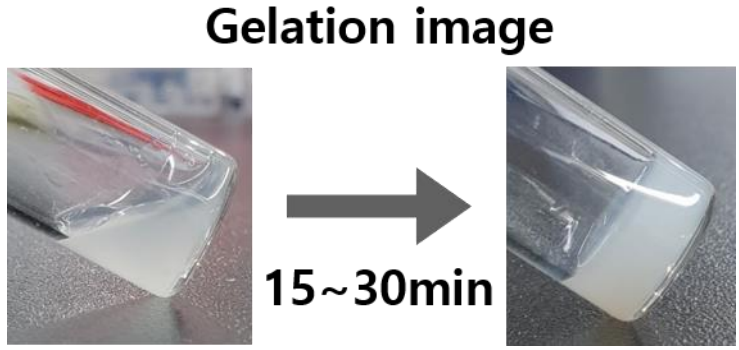

Figure 3.4. Gelation images of decellularized ECM hydrogel

Figure 3.5 Rheological analysis of decellularized ECM hydrogel

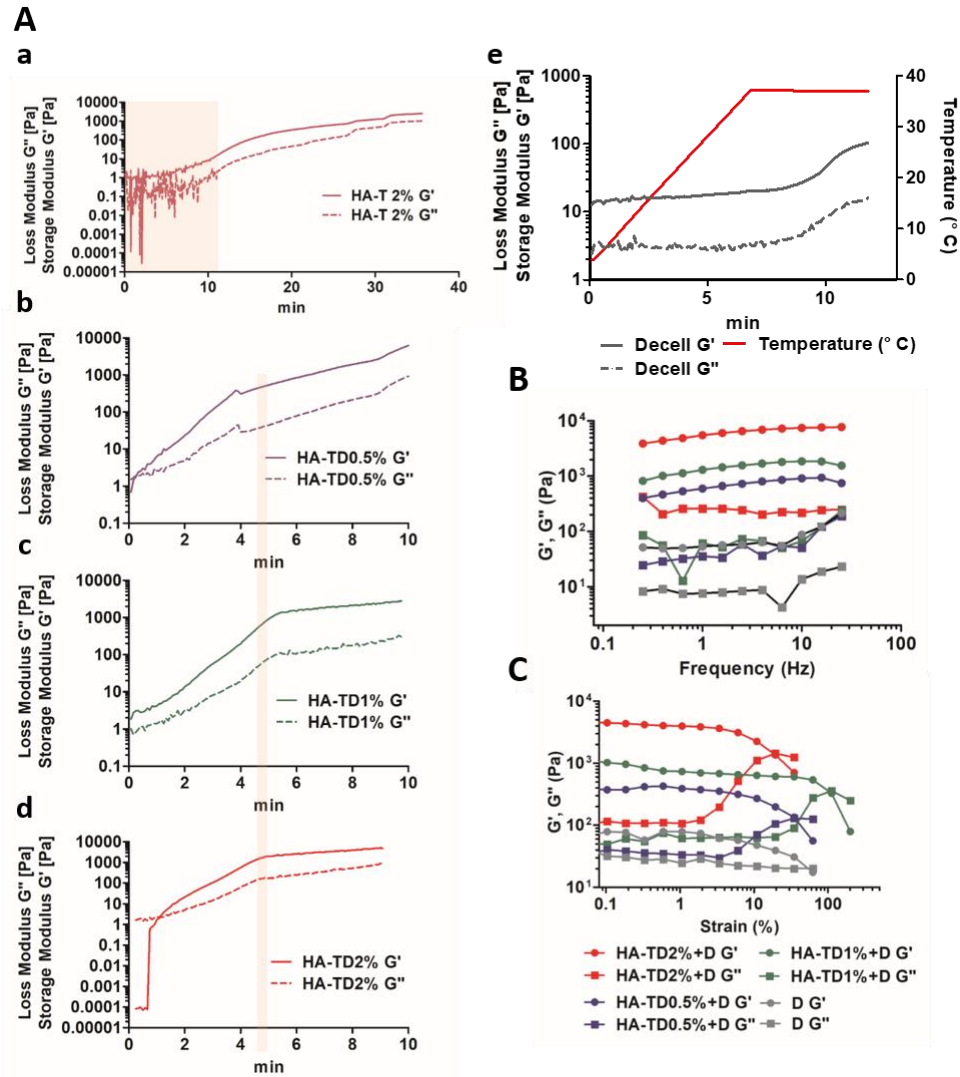

Figure 3.5. Rheological analysis of decellularized ECM hydrogel. (A) Time sweep test to verifying gelation time. a) HA_T 2% b) HA_TD 0.5% c) HA_TD 1% d) HA_TD 2% e) Decellularized ECM hydrogel with linear increases temperature from 4 to 37 °C (B) Frequency sweep test of hydrogel. (C) Shear strain test of the hydrogel.

Figure 3.6 Mechanical properties of decellularized ECM-based hydrogel

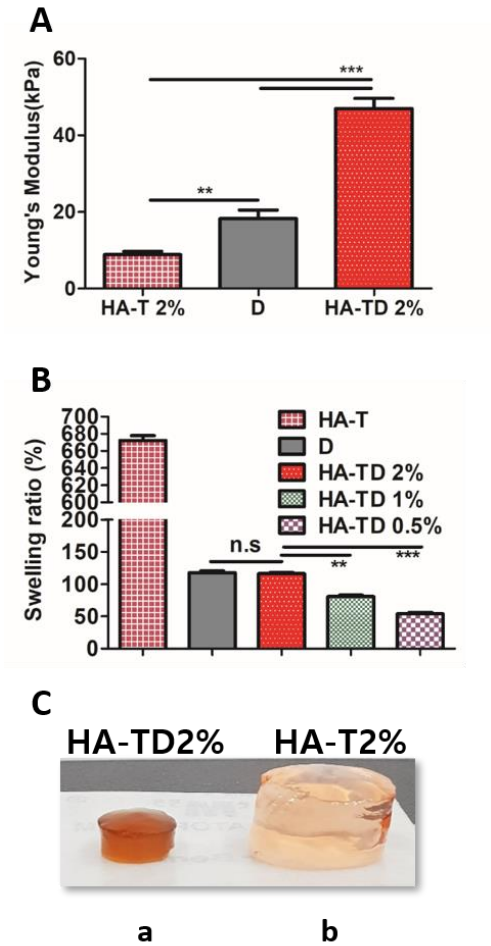

Figure 3.6. Mechanical properties of decellularized ECM-based hydrogel. (A) Young's modulus. n=3 (B) Swelling ratio. (C) Image after swelling HA-T2% and HA-TD2% hydrogel

Figure 3.7 Scanning electron microscope image

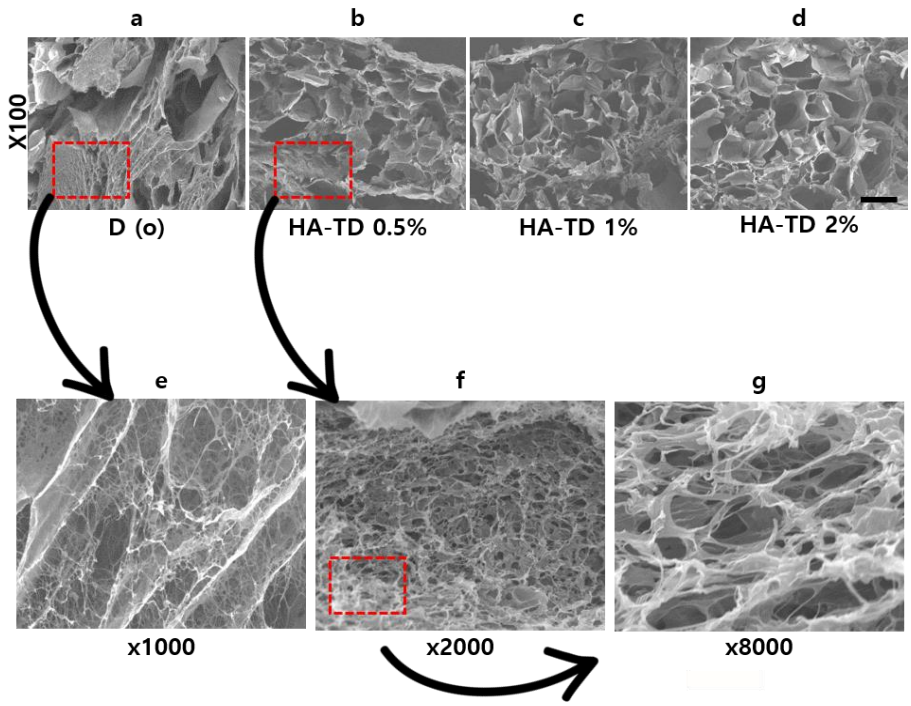

Figure 3.7. Scanning electron microscope image. a,e) Decellularized ECM hydrogel b,f,g) HA_TD 0.5% c) HA_TD 1% d) HA_TD 2%. Scale bar=100μm

Figure 3.8 Further work

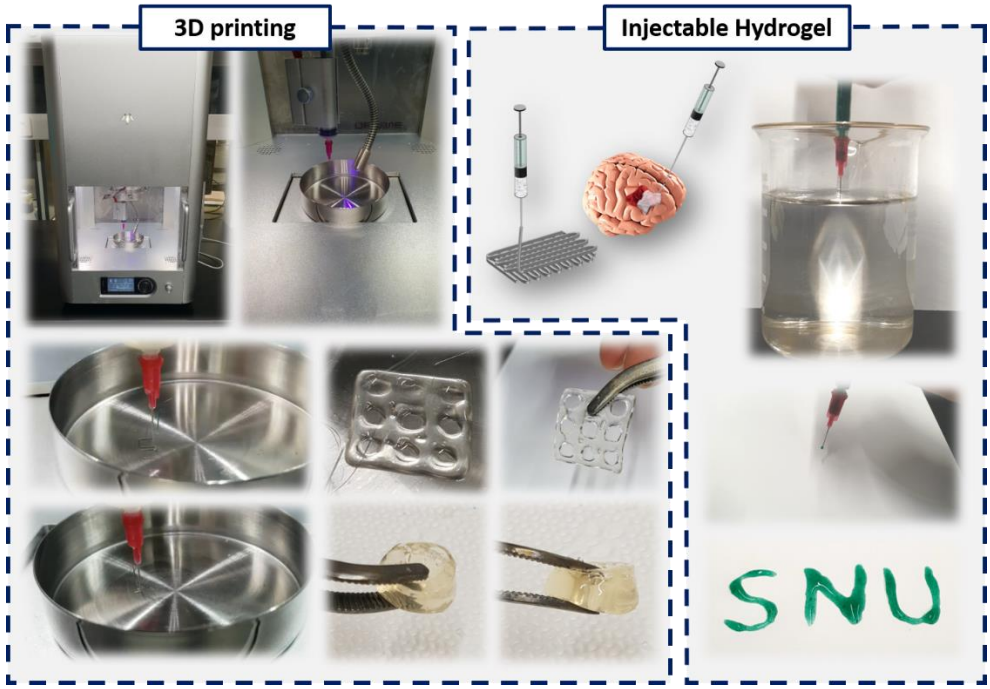

Figure 3.8. Decellularized ECM-based hydrogel that can be injectable and used for 3D printing.

Tables

Table 3.1 DNA quantification

Samples	DNA (ng) / dry weight (mg)	
Before	962.5 ± 11.66	
		-96%
After	38.92 ± 0.8661	

Table 3.1. DNA content before and after the decellularized process.

Table 3.2 Young's modulus of decellularized ECM-based hydrogel

Samples	E (kPa)
HA-T 2%	8.89 ± 0.83
D	18.29 ± 2.21
HA-TD 2%	46.99 ± 2.65

Table 3.2. Young's modulus of decellularized ECM-based hydrogel